Causal Computational Models for Gene Regulatory Networks

Sahil Loomba, Parul Jain

April 7, 2016

Abstract

Gene Regulatory Networks (GRNs) hold the key to understanding and solving many problems in biological sciences, with critical applications in medicine and therapeutics. However, discovering GRNs in the laboratory is a cumbersome and tricky affair, since the number of genes and interactions are very large, say for a mammalian cell. We aim to discover these GRNs computationally, by using gene expression levels as a "time-series" dataset. We research and employ techniques from probability and information theory, theory of dynamical systems, and graph structure estimation, to establish causal relations between genes, on synthetic datasets. Therefore, narrowing the space of genetic interactions to be looked at when discovering these GRNs in the lab.

Keywords: *gene regulation, network inference, causality, information theory, dynamical systems, random walk models*

Contents

1 Introduction

A single biological cell, is the basic independent building block of all lifeforms. Colloquially speaking, a cell is essentially a "bag" or membrane, enclosing a number of "chemicals" which govern the lower-level working (birth, survival, death) of the cell. These chemicals include mostly water, and proteins. Proteins themselves are created by a broadly two-step process of DNA transcription and translation. The DNA, as is common knowledge, is the storehouse of cellular information. Those sections of the DNA which code for important biomolecules such as proteins, are called **genes**. When a gene gets "activated", the process of transcription and translation ensues, leading to production of the relevant protein, in certain quantities and at certain points in time depending on the level of gene activation. For a graphical representation, see Figure 1. Genes themselves get activated through their interaction with proteins called **transcription factors**. This regulation can be either activating, or inhibitory. Some genes also undergo self-regulation, that is they regulate their own expression. (Although we ignore self-regulation for the purpose of our analysis.) Thus eventually, the expression of a gene of importance (GOI) is controlled by a usually large directed network of cascading gene interactions. It becomes very important to discover this network for the GOI not only so that we can model gene expression, but also so that we can better understand which regulatory pathways need to be targeted for therapeutics.

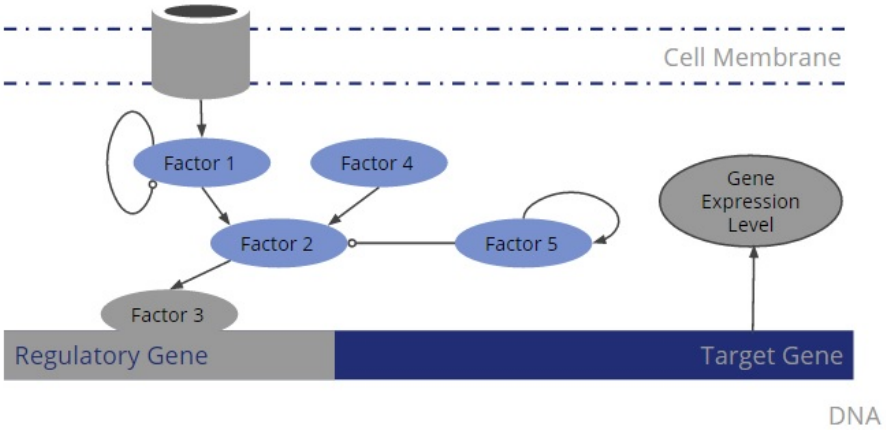

Figure 1: A cartoon representation of a Gene Regulatory Network. Each of the factors can be represented as nodes in a directed graph $G = \{V, E\}$

Since gene expression is temporal data, one could interpret the expression of genes connected in the GRN to be causally related signals. That is, if for two genes X and Y a directed regulatory edge exists from X to Y, then there exists a causal relation $X \to Y$. The problem of GRN discovery has thus been translated to a difficult problem of establishing causality between signals. We attempt to establish pairwise causality using various metrics, and thus arrive at conclusions as to which methods are favourable for this problem, and if at all establishing pairwise causality is sufficient for GRN discovery.

Reliable techniques to predict GRNs can help us understand physiological differences and predict/diagnose health issues. The biomarkers identified by such a method could be used to detect early onset of many diseases (Huntington, Alzheimer's etc). One could also imagine applications in therapeutics, since modelling of gene regulatory pathways and knockouts can allow us to design better-targeted drugs. Since the development of such a technique holds key to understanding multiple biological issues, there have been many attempts to solve the problem. Some of these are discussed in the sections that follow.

2 Previous Work

As discussed, the problem of GRN discovery is not a new one. Some of the current literature which has inspired our work is briefly discussed in the subsections that follow.

2.1 GRNs and their Applications

This paper is the motivation for our work and provides a general discussion and perspective on gene regulatory network [1]. GRNs represent statistically significant predictions of molecular interactions obtained from large-scale data. In other words, for genomes as large as that of humans, GRNs are of tremendous help in narrowing down **potential interactions** for which statistical support is available. Using prior knowledge about "partial" gene regulatory networks inferred from such observational data, we can have controlled experiments by establishing conditions that enhance molecular target processes to improve the signal strength. Since they consider the interaction structure between individual genes explicitly, GRNs could also be used as biomarkers, for diagnostic, predictive or prognostic purposes. As the number of discovered GRNs will grow, the comparison of networks will allow us to learn about interaction changes across different physiological or disease conditions and enrich our biological and biomedical understanding of various phenotypes. Most importantly, GRNs will enable production of personalised medicine as condition specific GRNs are closer to the phenotype than genetic or epigenetic markers.

After detailed analysis of the various methods used for GRN detection, the paper argues that results of such technical comparisons depend crucially on the **studied conditions**, including: type of data (simulated or real), size of the network, number of samples, amount of noise, experimental design (observational, experimental, interventional), type of the underlying interaction structure (scale-free, random, small-world) and error measure (global, local), among others. Also, though experimental research work and biological databases, used as ground truths, have a huge number of recorded interactions. Many of them might not be relevant to the biological conditions under investigation, which could affect truth assessment of the inferred network.

Keeping this in mind, parameters defining the data, used in the experiments for this project, were recorded in detail and underwent multiple perturbations so that the observations are not biased and results can be generalised. In addition, the experiments are performed on synthetic data for accurate evaluation of the performance with methods suggested in our work.

2.2 Discovering GRNs using Pairwise GC

This paper uses Granger Causality as the method of inference, but instead of using full model GC which considers all possible combinations, it considers pairs of genes at a time and only includes significant ones in the inferred network [2]. GC (see 4.3) is a "statistical concept of causality based on prediction" proposed by the Nobel laureate Clive Granger in Economics. However, pairwise GC produces large number of false edges. Thus, the first part of the paper is devoted to detecting the issues with pairwise GC and then, using techniques to reduce the number of **spurious edges**. The paper uses various methods to reduce the number of false edges. It first compares the performance on synthetic networks with and without the correction methods to establish their effectiveness. Then, it uses the method on human HeLa data-set.

It uses multivariate **autoregressive** model for data regression and uses F-statistic for significance. If the VAR model does not adapt to the data well, correlations between the variables cannot be captured properly and the GC detected is not reliable. There, model validation is done by checking model consistency, adjusted RSS and Durbin–Watson (whiteness) test. The model order is calculated through AIC or BIC and the network is inferred using both. Since BIC suits better where the data size is large, AIC was observed to produce better results on the HeLa data-set, which had a largest size of 47 only. Also, since there are ${}^nC_2$ pairs of genes for an n-variable network, there are as many p-values and hence the tests need correction, for which Bonferroni correction and Benjamini–Hochberg False Discovery Rate (FDR) controlling procedure are used.

On similar lines, our project uses pairwise GC as a method of inference. Since the size of time-series data is large (500, 1000), BIC is used for lag estimation. The paper concludes that though the accuracy of the method can not be estimated for real data sets, the techniques used could definitely make GC a strong contender for causality inference since correlation-based methods (such as Pearson correlation coefficient (PCC) and mutual information) cannot give direction of causality.

2.3 Information Theory for Causality Detection

The paper aims to provide a detailed overview of information theoretic approaches for measuring causal influence in multivariate time series, focusing on diverse approaches to entropy and mutual information estimation [3]. Natural phenomena emerge from complex systems which are composed of modules, interacting in a complex, often non-linear manner. The behavior of the system cannot be explained by a linear combination of the parts. Thanks to various databases, we now have big data representing the temporal dynamics of possibly interacting variables, but the methods which could make sense of the data are still being researched and developed. The paper suggests that information theory techniques are crucial to understanding such systems as they hold the key to causality detection which will help us understand the basic network structure of these system.

It explains causality under the Granger-Weiner framework and then extends it to non-linear systems, based on the information theoretic formulation of **transfer entropy** and **causal mutual information**. First, it lists the prerequisites for using entropy or mutual information for measurement, such as continuity, differentiability and boundedness, among others. Describing all the information theory methods in detail, it discusses the conditions under which they will be best suited. Finally, it discusses the idea of Granger Causality in detail along with its non-linear analogs. Hence, this paper provided a reference ground for selection of methods for information theory methods.

It argues that for a good entropy estimator, the condition of consistency seems to be important so that the method is applicable for the problem for a wide range of experimental conditions. This is essential as in case of biological systems, there are multiple genetic and epigenetic factors in play which control the data, making it bias in one way or another. Since truly generalized data is not feasible, consistency of method across conditions is desirable. With this, it agrees that conditional mutual information (or transfer entropy) is crucial to causality detection. Hence, we have used transfer entropy, suggested as the most promising method by the paper, along with mutual information for comparison of performance.

2.4 ARACNE

Considered to be state-of-the-art for inferring Gene Regulatory Networks, an Algorithm for the Reconstruction of Gene Regulatory Networks, or simply ARACNE, works on the metric of pairwise mutual information [4]. It defines an edge in the graph as an irreducible statistical dependency between gene expression profiles that cannot be explained as an artifact of other statistical dependencies in the network. It further propounds that there is no universally accepted definition of statistical dependencies in the multivariate setting.

Taking from literature on Markov networks, it represents a GRN as Markov network, and then defines clique potentials only till a pairwise level, ignoring higher order analysis. They then identify candidate interactions by estimating pairwise gene expression profile **mutual information**. Interactions are then filtered in two steps. First, using an appropriate thresholding, computed for a specific p-value, in the null hypothesis of two independent genes. Second, indirect interactions are detected using the **Data Processing Inequality** (DPI) which says that if two genes g_1 and g_3 can interact with each other only through a path via gene g_2 (that is, $g_1 \leftrightarrow ... \leftrightarrow g_2 \leftrightarrow ... \leftrightarrow g_3$), then $I(g_1, g_3) \leq min[I(g_1, g_2), I(g_2, g_3)]$.

The paper further claims (with proof) that if MIs can be estimated with no errors, then ARACNE reconstructs the underlying interaction network exactly, provided this network is a tree and has only pairwise interactions. It doesn't however comment on the validity of the assumption, in the first place. Thus, the real challenge of information theoretic measures lies in estimating probabilities, in the limit of poverty of data.

2.5 Benchmarking the methods

The paper [5] compares the performance of a method proposed by them, with popular network reconstruction methods including ARACNE. Our matter of interest is the datasets used by them for benchmarking:

1. A yeast time series data with over 5000 genes and close to 500 time series points
2. The first network of DREAM4 dataset, which is a network of size 10, with 105 time series points.

In our work, we use our own synthetic data (see Section 3) for doing pairwise analysis on large networks. We use the DREAM4 dataset for doing small scale analyses, and eventually the plan is to use the yeast dataset for a final large scale test of the entire model.

3 Datasets

The ultimate aim of this project requires us to work on real datasets for modelling and testing. However, most real datasets are very large in the number of genes and interactions. Therefore, we decided to start with synthetic datasets, generated using the MATLAB Toolbox called **SysGenSIM** [6].

The toolbox first generates a GRN topology, depending on: (a) number of genes, (b) average degree (c) a topology model (random, scale-free, modular, etc.) and (d) length of time series. We take these to be fixed parameters with respect to an experiment run, and use the scale-free topology. (See Figure 2 for an example network topology.) Then, it uses a non-linear ODE model given below, where the first term accounts for transcription, and the second term accounts for degradation.

$$\frac{\mathrm{d}\,G_g}{\mathrm{d}\,t} = Z_g^c \cdot V_g \cdot \theta_g^{syn} \cdot \prod_k \left(1 + A_{k,g} \frac{G_k^{h_{k,g}}}{G_k^{h_{k,g}} + (K_{k,g}/Z_k^t)^{h_{k,g}}}\right) - \lambda_g \cdot \theta_g^{deg} \cdot G_g$$

Where G_g is mRNA concentration of gene g which is the gene of interest, V_g is its basal transcription rate, and λ_g is the degradation rate constant. The G_k are expression levels of genes which have directed edges into node i.e., the genes that affect the expression of gene G_g. $K_{k,g}$ is the interaction strength, a Michaelis constant (non-negative, denoting how strongly does gene G_k affect G_g), $h_{k,g}$ is a cooperativity coefficient (and controls the extent of non-linearity of the interaction), and $A_{k,g}$ is an element of matrix A encoding the signed network structure representing the kind of effect (-1 for inhibitor, 1 for activator, 0 for no effect). The biological variance parameters θ_g^{syn} and θ_g^{deg} represent non-genetic additional biological noise in the transcription and degradation rates, respectively, and are sampled from a normal distribution with unit mean and user specified standard deviations. This is to ensure that the data is closer to what is observed in the real world with respect to error reporting. Z_g^c and Z_k^t are parameters that incorporate effects of DNA variants and represent the effect on the transcription rate of G_k when the variant is in its own promoter region or in the coding region of its regulatory gene respectively.

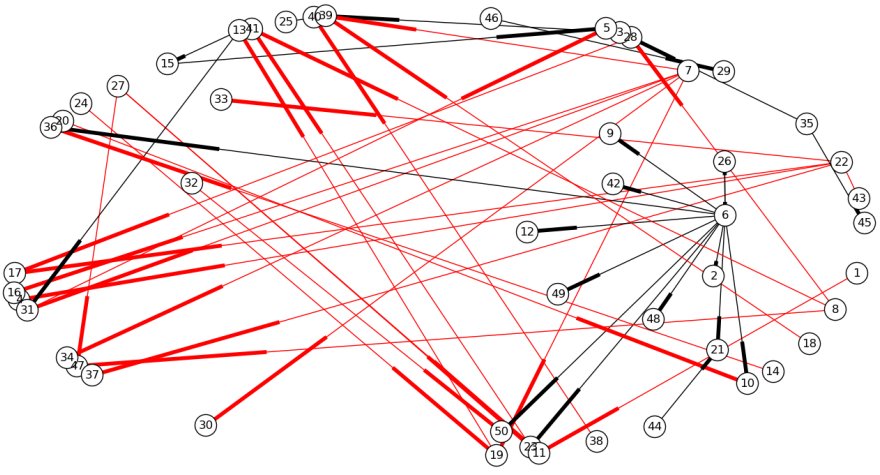

Figure 2: An example network topology with 50 nodes. Notice the scale-free distribution followed by the network: few nodes with high degree, many nodes with low degree.

The data output of SysGenSIM is essentially a time-series matrix of size $N \times T$ for N genes and T time steps. We obtain these datasets for $N \in \{10, 20, 50, 100\}$ and for $T \in \{500, 1000\}$. Moreover, every dataset was quantised to different levels of quantisation, $Q \in \{2, 5, 10, 20\}$ for the probabilistic

techniques. See Figure 3 for a visualisation of the effect of quantisation on signal space. And, as is standard practice, the data was normalised to zero mean and unit variance.

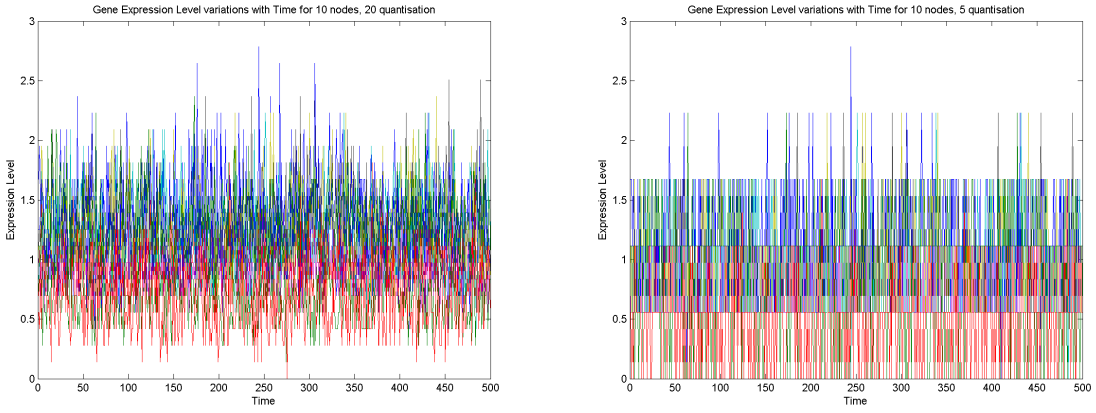

(a) $Q = 20$ (b) $Q = 5$

Figure 3: An example of signal quantisation for GRN with $N = 10$

4 Pairwise Metrics

One of the two core approaches in our work is to look at signals in a pairwise fashion, and then use a metric which works as a thresholding function from "non-causal" to "causal" relation. Here, we work with primarily six methods (or *metrics*), first four of which treat gene expression levels (time-series signal) for a given gene G, as a random variable X, coming from an underlying probability distribution $P(X)$. For a summary of methods, see Figure 5.

4.1 Correlation

Correlations are used to measure the notion of co-dependence between two signals. More specifically, a linear correlation can be used to find existence of simple linear relationships between these signals. We use the unsigned value of the Pearson Correlation Coefficient (PCC) $\rho(X, Y)$ to quantify this linear correlation. In its most concise statistical form, PCC can be expressed as:

$$\rho(X, Y) = \frac{cov(X, Y)}{\sigma_X \sigma_Y}$$

Where $cov(X, Y)$ refers to the covariance between signals X and Y, and σ_X refers to the variance in signal X. This can be expanded further to express them in terms of probability distributions which govern the two signals, which have been assumed to be random variables. For visual acuity, we write only the unstandardised PCC, i.e. the covariance, in terms of probabilities.

$$\begin{aligned} cov(X, Y) &= E[XY] - E[X]E[Y] \\ cov(X, Y) &= \sum_{x,y} xyP(x, y) - \sum_x xP(x) \sum_y yP(y) \\ cov(X, Y) &= \sum_{x,y} \big(P(x, y) - P(x)P(y)\big)xy \end{aligned} \tag{1}$$

Some key mathematical properties of PCC are:

- It is symmetric in X and Y, which does not capture a sense of direction in causality. However, we make use of (maximum) shifted correlation, and on the basis of the sign of shift (positive/negative), we decide the direction of causality.
- Its value ranges between -1 and 1, with values close to zero implying low correlation and those close to ± 1 implying high (positive/negative) correlation.
- It captures linear relations. The square of the PCC is same as the coefficient of determination r^2 when trying to do a linear regression between the two signals. Thus, a value of zero means a lack of *linear* relationship.
- Clearly, there is no sense of predictability or causation, but mere co-dependence. Hence the common but appropriate adage "correlation does not imply causation".

4.2 Mutual Information

In the purview of statistical theory, Mutual Information or MI captures non-linear correlations between signals. In information theory, MI is a measure of how much extra information can a given signal Y provide about another signal X. In its most concise information theoretic form, MI can thus be expressed as:

$$I(X, Y) = H(X) - H(X|Y)$$

Where $H(X)$ refers to the entropy of X, and $H(X|Y)$ is the conditional entropy of X given Y. Expressing these quantities in terms of probability distributions of the two random variables, it can be

shown that MI captures their mutual dependence. That is, it quantifies how close the joint distribution of the two signals is to the product of their marginal distributions.

$$I(X,Y) = E\left[log\left(\frac{P(x,y)}{P(x)P(y)}\right)\right]$$

$$I(X,Y) = \sum_{x,y} log\left(\frac{P(x,y)}{P(x)P(y)}\right)P(x,y)$$

$$I(X,Y) = \sum_{x,y} \Big(log\big(P(x,y)\big) - log\big(P(x)P(y)\big)\Big)P(x,y) \tag{2}$$

Looking at equations 1 and 2 together offers some insight into how correlation and mutual information convey the relationship between the signals X and Y. While the former creates a weighted sum of product of signal values, the latter generates a weighted sum of joint probabilities.

Some key mathematical properties of MI are:

- It is symmetric in X and Y, which does not capture a sense of direction in causality.
- Larger is the value of mutual information, higher is the mutual dependence between the two signals.
- It does not concern itself with the linearity of the signals involved, since it only worries about the probability distribution of the two signals. But evaluating these distributions accurately is significantly more challenging than calculating a simple PCC.

4.3 Granger Causality

Given by the British economist Clive Granger, Granger Causality is a statistical test to determine whether a time signal can help forecast another time signal [7]. Thus, this test can be used to confirm only the idea of "predictive causality". A signal Y is said to Granger cause another signal X if the prediction of future values of X based on its own as well as Y's past values is "more accurate" than that based on X's past values alone.

Essentially, GC is an F-test, where the test statistic (an attribute of a sample) follows the F-distribution. This distribution is parametrised by two quantities d_1 and d_2, such that its random variate Z can be expressed in the form $Z = \frac{W_1/d_1}{W_2/d_2}$, where W_1 and W_2 are random variables following the chi-squared distribution parametrised by d_1 and d_2 degrees of freedom respectively. The random variate of a chi-squared distribution W can itself be expressed in the form $W = \sum_{i=1}^{d} X_i^2$, where X_is are independent normal random variables.

From here, it is easy to see how an F-test can be applied to estimate GC. We define predictability in the sense of how closely previous values can be used to fit the future value of a time signal. Thus, in the "restricted model" M_1, we have an autoregression of X given by

$$x_t = a_0 + \sum_{i=1}^{m} a_i x_{t-i} + \epsilon_t$$

In the "unrestricted model" M_2 we append this autoregression with past values of Y as

$$x_t = a_0 + \sum_{i=1}^{m} a_i x_{t-i} + \sum_{i=1}^{q} b_i y_{t-i} + \epsilon_t$$

We can now define the F-statistic for determining goodness of fit as the following, using the Z representation given above, where RSS refers to the residual sum of squared errors, p_i refers to number of parameters of model i, and n is total number of data points:

$$F(X,Y) = \frac{\left(\frac{RSS_1 - RSS_2}{p_2 - p_1}\right)}{\left(\frac{RSS_2}{n - p_2 + 1}\right)}$$

$$F(X,Y) = \frac{\left(\frac{RSS_1 - RSS_2}{q}\right)}{\left(\frac{RSS_2}{n-(m+q+1)}\right)} \tag{3}$$

The null hypothesis for this test says that Y does not Granger cause X. Thus, larger is the value of this F-statistic, the more likely we are to reject this hypothesis. Thus, we reject it when $F(X,Y)$ is more than the critical value of the F-distribution parametrised by q and $n-(m+q+1)$, for some desired false-rejection probability α like 0.05.

Some key mathematical properties of GC are:

- It is asymmetric in X and Y, which captures a sense of direction in causality.
- Larger is the value of the F-statistic, higher is the predictive causality from Y to X.
- It assumes the causal relationship between two signals to be linear, since the autoregression is linear and not polynomic.

4.4 Transfer Entropy

In probability and information theory, Transfer Entropy refers to the amount of information transfer between two random processes. In words, it measures something similar to GC, that is, it quantifies the reduction in uncertainty of future values of X, by knowing past values of Y, given past values of X. In another sense, it is nothing but the conditional mutual information of X and Y, given past values of Y. If d is the lag assumed, then it is given by:

$$T(X,Y) = T_{Y\to X} = H(X_t|X_{t-1:t-d}) - H(X_t|X_{t-1:t-d}, Y_{t-1:t-d})$$

Assuming a lag of 1 unit in the simplest case, we can write $T(X,Y)$ as:

$$T(X,Y) = T_{Y\to X} = \sum_{x_{t+1},x_t,y_t} \Big[log\big(P(x_{t+1},x_t,y_t)P(x_t)\big) - log\big(P(x_t,y_t)P(x_{t+1},x_t)\big)\Big] P(x_{t+1},x_t,y_t) \tag{4}$$

- It is asymmetric in X and Y, which captures a sense of direction in causality.
- Larger is the value of transfer entropy, higher is the information transfer between the two signals (or "processes").
- It does not concern itself with the linearity of the signals involved, since it only worries about the probability distribution of the two signals. But evaluating these distributions accurately is significantly more challenging, since usually long time series data is required.
- For auto-regressive processes, Transfer Entropy has been shown to reduce to Granger Causality.

4.5 Aside on Laplace Smoothing

One key issue with using gene expression time-series data, is that most real datasets are recorded over a very small span of time, say around a thousand time-steps. Depending on the domain of the time signal X, assuming it's discrete given some least count of measurement, one could imagine that evaluating probabilities over a larger domain/sample space would require a larger amount of data. Also, the more the number of variables in a joint distribution, the larger the sample space of the distribution becomes. Looking at the expressions for the four methods above, it becomes clear that the probability estimates from the data alone, may not be close to the true probabilities.

In such cases, we can do what is called "smoothing" of the data. Say we are given counts over a sample space $S = (s_1, s_2, ..., s_n)$ of size n as $(c_1, c_2, ..., c_n)$, total count C, one could find the probability distribution parameters as:

$$\theta_i = \frac{c_i + \alpha}{C + \alpha n}$$

If $\alpha = 0$, there is no Laplace Smoothing. In practice, α is kept at a small value less than or equal to 1. We keep it as unity for our analysis.

4.6 Convergent Cross Map

All four methods listed above, treat time-series signals as being random variables with some underlying probability distributions. However, there is another picture of looking at a time-series signal: as it being a part of some dynamical system. A dynamical system represents the temporal evolution of a signal in geometric space, often called the manifold representation of the system. The assumption is no longer of randomness, rather, of a deterministic system, which has the potential for showing unpredictable behaviour, often termed as "chaotic" behaviour.

Consider two time-series signals X and Y belonging to the same dynamical system represented by the manifold M of dimension d. Since we are dealing with non-linear biological systems, we assume A non-linear dynamical system. Mathematically, we can express the manifold as:

$$M(t) = [X(t), Y(t), ...]$$

We can now define something called a "shadow manifold" with respect to one of the signals, say $M_X(t)$ constructed by time-lagged (τ-lagged) values of X. We assume $M_X(t)$ to have a dimensionality E no less than that of M, that is, $d \leq E$, and given by:

$$M_X(t) = [X(t), X(t-\tau), ..., X(t-\tau(E-1))]$$

Now, using Taken's embedding theorem, one can reconstruct M from M_X, since there exists a one-to-one correspondence between the true manifold M and the shadow manifold M_X (that is, they are diffeomorphic). Similarly, one can say that M_Y is diffeomorphic to M, and thus, the two shadow manifolds are diffeomorphic to one another. Because X and Y are dynamically coupled, points that are nearby on M_X will correspond temporally to points that are nearby on M_Y (see Figure 4). This enables us to estimate states across manifolds using Y to estimate the state of X and vice-versa using k-nearest neighbours [8]. With longer time series, the shadow manifolds become denser and the neighbourhoods shrink, allowing more precise cross-map estimates.

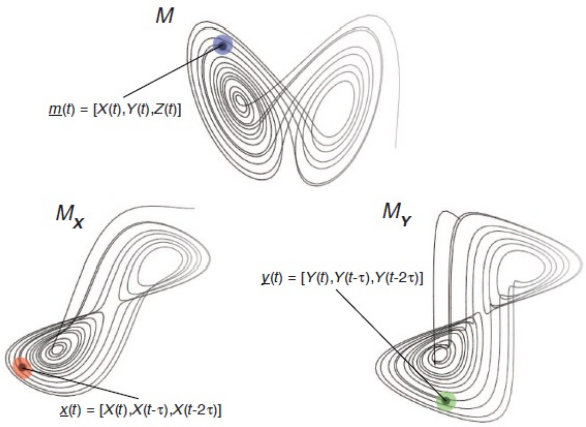

Figure 4: A sketch showing the attractor manifolds: true manifold M and shadow manifolds M_X and M_Y, with a diffeomorphism across all three [8].

Thus, without loss of generality, if $\hat{X}_Y$ be the reconstruction of signal X from shadow manifold M_Y, then a qualitative degree of causality using CCM can be given by the PCC between the two. That is, to test for $X \to Y$, we find

$$C(X, Y) = \rho(X, \hat{X}_Y) \tag{5}$$

Note that although the direction of causality might appear counterintuitive, CCM says that if $X \to Y$, then a signature of X must be contained in Y. Some mathematical properties of CCM are:

- It is asymmetric in X and Y, which captures a sense of direction in causality.
- Larger is the value of correlation between original and reconstructed signals, higher is the degree of causality between the two signals.
- It does not assume linearity of the system.
- Longer is the time-series, larger is the "library size", denser is the manifold, smaller is the neighbourhood, and higher is the precision in establishing causality.
- Although not entirely a substitute for other metrics like GC, CCM has been shown to work well for weakly coupled systems.

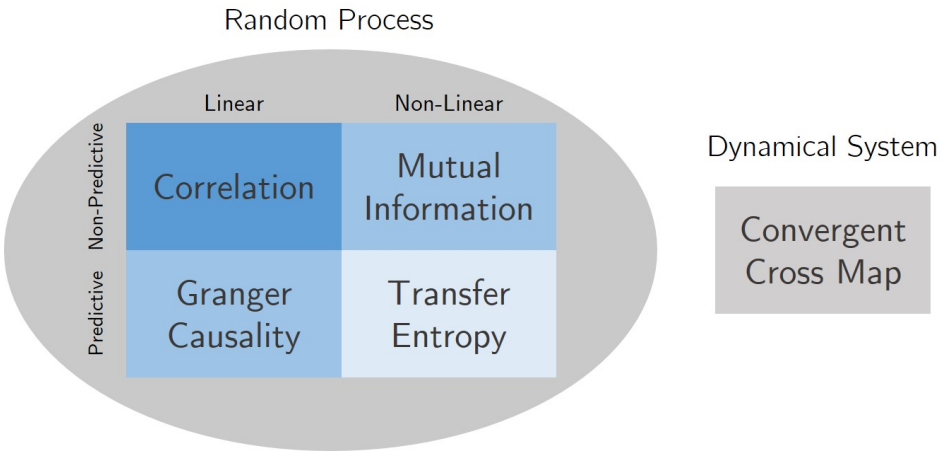

Figure 5: A succinct graphical summary of the methods used for estimating pairwise causality between signals X and Y.

5 Intrinsic Graph Estimation

The other of the two core approaches in our work is to look at global causal computational models of a gene regulatory network. Clearly, using just pairwise metrics for determining the entire causal model is a naive strategy, wherein since all pairwise metrics are directly proportional to the strength of causality, this algorithm works: (1) sort ${}^nC_2$ edges by metric value in decreasing order, (2) choose top-k edges and output as graph G. However, one could imagine a more sophisticated algorithms to come up with this ordering. One, which also looks at higher order interactions between the nodes of the graph, by taking the original pairwise metric matrix as an input. ARACNE is one simple yet powerful algorithm which looks at small higher order interactions (like the DIP inequality), however, we'd like to look at all possible interactions in the graph. Taking forward from the work of Noda et al. [10], we present the method of intrinsic graph estimation.

Let us call the given pairwise metric matrix Ξ (called the observation matrix), and the underlying graph structure (what we have to discover) represented by its adjacency matrix Θ. One can now imagine a mapping f which captures how observed data (gene expression modality such as one or more of the pairwise metrics) rises from the network structure (see Figure 6a). That is:

$$f : \mathbb{R}^{n\times n} \to \mathbb{R}^{n\times n}$$

$$\Theta \mapsto f(\Theta) = \Xi$$

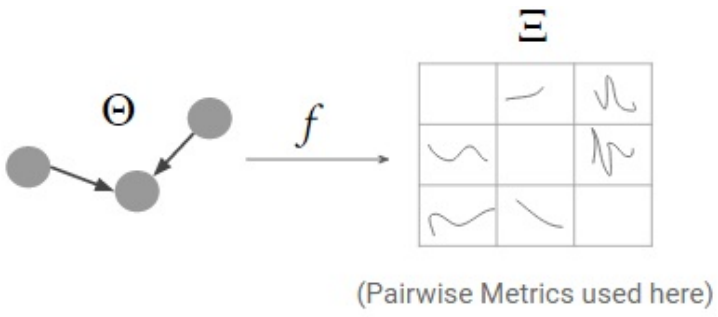

(a) f maps from graph structure to observation matrix

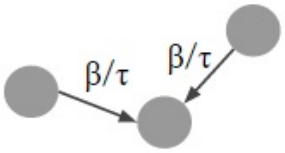

(b) Random walk model for modelling network interactions

Figure 6: Schematics of intrinsic graph estimation for single-attribute observation matrix

Now, we are in a position to explicate the network interactions. The assumption is that the observation matrix can be obtained as a weighted linear contribution of multiple-order interactions in the network structure. That is,

$$\xi_{ij} = \underbrace{c_i}_{\text{zero-order}} + \overbrace{c_{ij}\theta_{ij}}^{\text{first-order}} + \underbrace{\sum_{k\in V} c_{ij}^{k}\theta_{ik}\theta_{kj}}_{\text{second-order}} + \overbrace{\sum_{k,l\in V} c_{ij}^{kl}\theta_{ik}\theta_{kl}\theta_{lj} + \dots}^{\text{higher-order interactions}}$$

Also, every observation datum has some additive natural noise, which could be Gaussian.

$$t_{ij} = \xi_{ij} + \epsilon \text{ where } \epsilon \sim N(\mu, \sigma^2)$$

Ultimately, the objective of intrinsic graph estimation (IGE) would be do find the constants c. To do that, we need to have a notion of error which we would like to minimise, so that these constants best fit the observed data for given structure Θ. This can simply be the squared error, given by the following, where ρ are the parameters of f (or the constants of the interaction model described above):

$$J(\rho, \Theta) = \sum_{i,j \in V, i \neq j} \Big(t_{ij} - [f(\Theta)]_{ij} \Big)^2$$

However, notice that the structure Θ is not exactly given. Therefore, we must estimate the structure simultaneously with the parameters of the model. This is a typical EM-Algorithm style setting where we can have the following:

$$\text{E step: } \Theta = f^{-1}(\Xi)$$

$$\text{M step: } \rho = \underset{\rho}{\operatorname{argmin}}\, J(\rho, \Theta^m)$$

Before we go on to describe the algorithm, it's important to explicate which mathematical functions are a good candidate for f. To understand that, we will describe this problem by a **random walk model** on the graph Θ. If $\beta \in \mathbb{R}$ be the transition probability in a short interval $1/\tau$ (see Figure 6b), then (check for yourself that) the probability matrix for this interval can be written simply as $I_n - \frac{\beta}{\tau} L(\Theta)$, where the digraph Laplacian is given by

$$L(\Theta) = \begin{bmatrix} \sum \theta_{1k} & -\theta_{12} & \dots & -\theta_{1n} \\ -\theta_{21} & \sum \theta_{2k} & \dots & -\theta_{2n} \\ \vdots & \vdots & \ddots & \vdots \\ -\theta_{n1} & -\theta_{n2} & \dots & \sum \theta_{nk} \end{bmatrix}$$

Now, if we look at the τ-step probability matrix, then on considering the continuous time limit of the random walk, we get the transition probability matrix as:

$$\lim_{\tau \to \infty} \left(I_n - \frac{\beta}{\tau} L(\Theta) \right)^{\tau} = e^{-\beta L(\Theta)} \text{ ; where } e \text{ refers to the matrix-exponential map}$$

Now, by appending a positive multiplicative term $\alpha \in \mathbb{R}_+$, one can compare this to the interaction model described above, and thus a good candidate function f can be:

$$f(\Theta; \alpha, \beta) = \alpha e^{-\beta L(\Theta)} \text{ and } \rho = \{\alpha, \beta\}$$

And f^{-1} can be given by the matrix-logarithmic map, that is:

$$[log \Xi]_{ij} = [log(\alpha I) - \beta L(\Theta)]_{ij} = \begin{cases} log\alpha - \beta \sum_{k \in V} \theta_{ik}, & i = j \\ \beta \theta_{ij} & i \neq j \end{cases}$$

Thus, graph structure can be estimated as:

$$\theta_{ij} = \frac{[log \Xi]_{ij}}{\beta} \text{ ; for } i \neq j$$

Given the mathematical background given above, we describe the algorithm below [1]. Note that while estimating the parameters Θ and ρ, we also need to update the diagonal elements of Ξ, which are otherwise undefined.

5.1 Incorporating a Multi-attribute Observation Matrix

At times, one might be dealing with a multi-attribute observation matrix. That is, the graph structure could be giving rise to more than one observable phenomenon. Say in our case, it could be "correlative" phenomenon, "Granger causal" phenomenon, "CCMic" phenomenon, etc. How do we account for all of these observations from the same structure matrix Θ? One could imagine taking a weighted linear combination of all these features to form a single-attribute matrix, like we had in the original case. However, this proposes a critical issue. Up until now, IGE had a great advantage: it was a **parameterless model**, which means it didn't require any parameter tuning whatsoever. However,

Algorithm 1 Intrinsic Graph Estimation for Single-attribute Data

Input: Metric matrix $T \in \mathbb{R}^{n \times n}$, maximum iterations k'
$\Xi = T + rI_n$ ▷ Where r is such that $|\Xi| \neq 0$ so that matrix-log exists
for $m = 1$ to $n(n-1)$ **do** ▷ Iterating over best networks for m edged networks
  for $k = 1$ to k' **do**
    $[\hat{\Theta}]_{ij} = \begin{cases} 1, & |[log\Xi]_{ij}| \geq \zeta_m \text{ and } i \neq j \\ 0, & \text{otherwise} \end{cases}$ ▷ Thresholding to select top-m edges
    $\rho^m = \text{argmin}_\rho \, J(\rho, \Theta^m)$ ▷ Find optimal parameters $\rho = (\alpha, \beta)$
    $\Xi = T + diag(\alpha^m e^{-\beta^m L(\Theta^m)})$ ▷ Update diagonal elements of metric matrix
$\hat{m} = \text{argmin}_{m \in \{1,2,\ldots n(n-1)\}} \, J(\rho^m, \Theta^m)$
return $\hat{\Theta}^m$

feature weighting would require us to tune these weights prior to applying IGE, that would amount to learning them under a supervised learning paradigm, which brings us back to the issue of paucity of data. To keep our methods parameterless and unsupervised, we propose the following extension.

We concatenate individual observation matrices to form a multi-attribute observation matrix, and thus can rewrite what we wrote for the single-attribute case as below, defining map g as (see Figure 7):

$$g : \mathbb{R}^{n \times n} \to \mathbb{R}^{n \times n \times s}$$

$$\Theta \mapsto g(\Theta) = \Xi$$

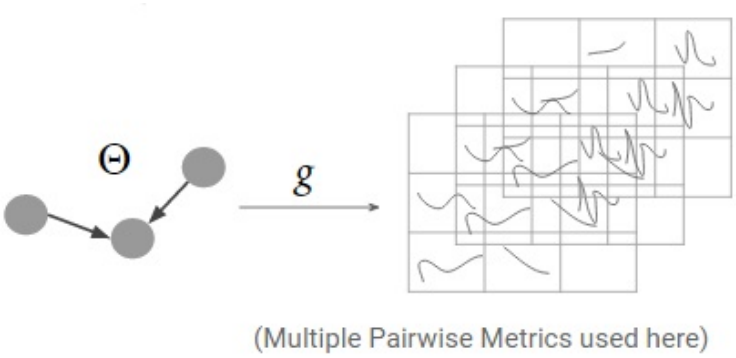

Figure 7: Schematic of intrinsic graph estimation for multi-attribute observation matrix

We can write the interaction model as:

$${}^q\xi_{ij} = {}^qc_i + {}^qc_{ij}\theta_{ij} + \sum_{k \in V} {}^qc^k_{ij}\theta_{ik}\theta_{kj} + \sum_{k,l \in V} {}^qc^{kl}_{ij}\theta_{ik}\theta_{kl}\theta_{lj} + \ldots$$

$${}^qt_{ij} = {}^q\xi_{ij} + \epsilon$$

The error function can be written as:

$$\tilde{J}(\rho, \Theta) = \sum_{1 \leq q \leq s} \left(\sum_{i,j \in V, i \neq j} \left({}^qt_{ij} - {}^q[g(\Theta)]_{ij} \right)^2 \right)$$

Now however, one might ask which function is a good candidate for g. So as to not abandon the advantages of using an elegant random walk model, let us try to incorporate the function f we defined above, and define g as:

$$g(\Theta) = cat\big({}^1f(\Theta), {}^2f(\Theta), \ldots, {}^sf(\Theta)\big) = \Xi$$

We now define the inverse map h:

$$\Theta = h\big({}^1f^{-1}({}^1\Xi), {}^2f^{-1}({}^2\Xi), \ldots, {}^sf^{-1}({}^s\Xi)\big)$$

There are more than one choices for the function h, as long as it as an aggregate-of-sorts of the network structures predicted by a single-attribute matrix alone. Thus, we have chosen the logical-and operator, while ensuring that the number of edges is limited to m in the m^{th} iteration.

$$h(x_1, x_2, \ldots, x_s; m) = \{x_1^{m'} \wedge x_2^{m'} \cdots \wedge x_r^{m'} : \text{for smallest } m' > m \text{ such that number of edges is } m\}$$

The final algorithm is described below 2.

Algorithm 2 Intrinsic Graph Estimation for Multi-attribute Data

Input: Metric matrix $T \in \mathbb{R}^{n \times n \times s}$, maximum iterations k'
$\Xi = T + rI_n$ ▷ Where r is such that $\forall q \in \{1, 2, \ldots, s\}$, $|{}^q\Xi| \neq 0$ so that matrix-log exists
for $m = 1$ to $n(n-1)$ **do** ▷ Iterating over best networks for m edged networks
  for $k = 1$ to k' **do**
    $m' = m$
    while true **do**
      $\hat{\Theta} = ones(n, n)$ ▷ Initialised to all 1s
      for $q = 1$ to s **do**
        $[{}^q\hat{\Theta}]_{ij} = \begin{cases} 1, & |[log\Xi]_{ij}| \geq \zeta_{m'} \text{ and } i \neq j \\ 0, & \text{otherwise} \end{cases}$ ▷ Thresholding to select top-m' edges
        $\hat{\Theta} = \hat{\Theta} \wedge {}^q\hat{\Theta}$
      if $sum(\hat{\Theta}) = m'$ **then**
        break
      else
        $m' = m' + 1$
    $\rho^m = \text{argmin}_\rho \tilde{J}(\rho, \Theta^m)$ ▷ Find optimal parameters $\rho = (\alpha, \beta)$
    for $q = 1$ to s **do**
      ${}^q\Xi = {}^qT + diag({}^q\alpha^m e^{-{}^q\beta^m L(\Theta^m)})$ ▷ Update diagonal elements of metric matrix
$\hat{m} = \text{argmin}_{m \in \{1,2,\ldots n(n-1)\}} \tilde{J}(\rho^m, \Theta^m)$
return $\hat{\Theta}^m$

5.2 Penalty on highly connected networks - Regularisation

When a plot of the variation of error for the best Θ^m versus m is made, it is realised that the error values for highly connected networks is quite low, compared to those of sparser networks, for most observation matrices. (See Figures 8 and 9 below.) Thus, our current error function mostly tends to favour denser networks, which could be problematic for natural biological networks like GRNs, which are quite sparse. Thus, we can introduce a simple regularisation to the error function, as below:

$$\hat{J}(\rho, \Theta) = J(\rho, \Theta) + \lambda \sum_{i,j}^{n} \theta_{ij}$$

Notice, however, that this forces the introduction of a parameter λ to an otherwise parameter-less model, which reduces the elegance of our model for better accuracy. Thus, perhaps an entirely different error function which naturally favours sparser networks can be imagined, which keeps IGE parameterless.

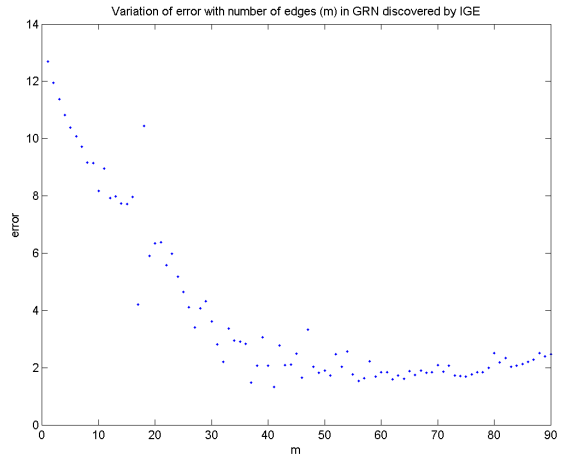

(a) Correlation

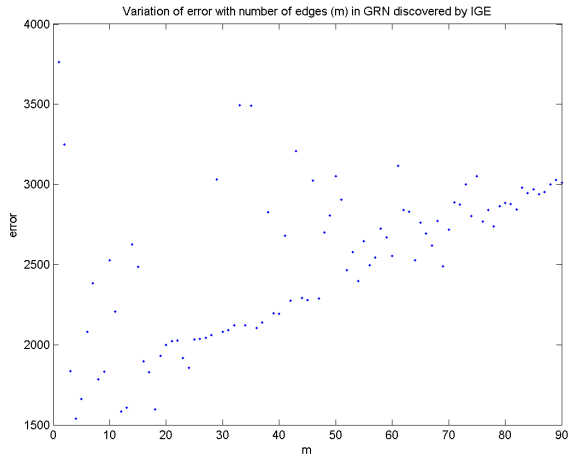

(b) Granger Causality

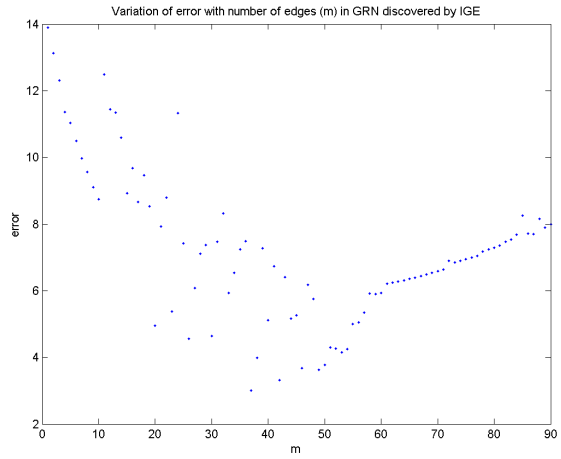

(c) Convergent Cross Map

Figure 8: Variation in error with number of edges for IGE in DREAM4 dataset: 15 true edges

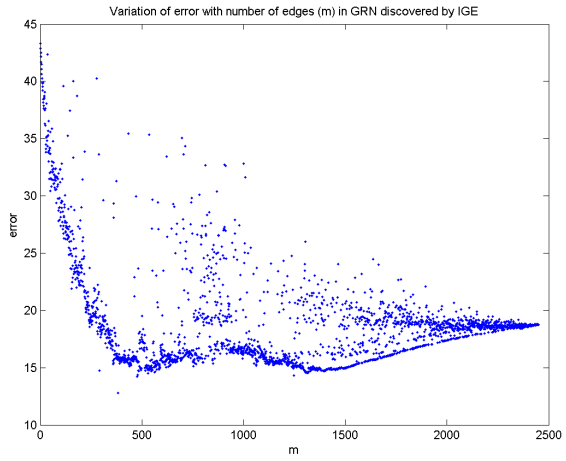

(a) Correlation

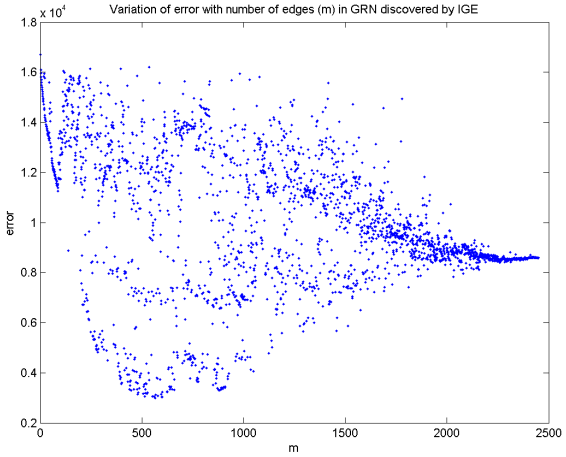

(b) Granger Causality

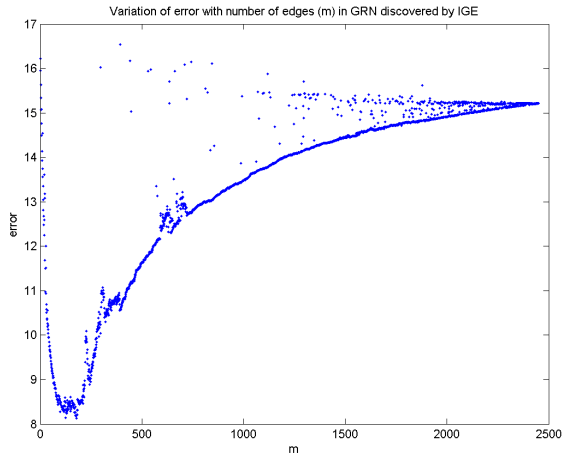

(c) Convergent Cross Map

Figure 9: Variation in error with number of edges for IGE in dataset: $N = 50$, $T = 1000$, 50 true edges

6 Experiments and Results

6.1 Time Lag of Causal Relation

An important parameter in establishing causality between two signals is the time scale over which causality operates, that is, the **"time lag"** to be considered. Firstly, a hyperparameter called "max lag" was defined, and set to 5, such that the optimum lag chosen does not exceed it. For correlation, mutual information and transfer entropy, the optimum lag was assumed to be "optimistic", in the sense that the lag giving the largest metric value for that pair of signals, was chosen for them. For Convergent Cross Map, this was taken as unity. For Granger Causality, an information theoretic criterion, called the Bayesian Information Criterion (BIC) was used [9]. BIC trades off the model complexity with the likelihood of the model, and is given by:

$$BIC = -2 \cdot ln(L) + k \cdot ln(n)$$

Where k is number of parameters, and n is number of data points. For GC, this can be written in terms of RSS as:

$$BIC = n \cdot ln(RSS/n) + k \cdot ln(n)$$

And then, the time lag which gives the smallest BIC is chosen as the optimal lag.

6.2 Result Metrics

The observations are interpreted using four metrics of performance.

- **Precision** is defined as the fraction of retrieved data that is accurate. It tells us what fraction of the detected data is actually correct. It is measured as the ratio of number of correct edges detected (*true positive*) to the total number of edges in the inferred network (*test positive*).

  $$precision = \frac{true\ positive}{test\ positive}$$

  Higher the value of precision, more is the "goodness" of the inferred network.

- **Recall** is the fraction of accurate data that was retrieved by the method. It represents the fraction of the true data that the method was able to successfully detect and it is measured as the ratio of edges detected correctly (*true positive*) to the number of edges in the real network (*condition positive*).

  $$recall = \frac{true\ positive}{condition\ positive}$$

  It denotes the coverage of the network by the method.

- **F-score** can be interpreted as a weighted average of the precision and recall, where an F-score reaches its best value at 1 and worst at 0. High precision could also be obtained due to a small number of edges getting successfully detected with most of the true edges getting rejected (*false negatives* or Type II error). Similarly, high recall may be obtained by selecting all the possible edges, most of which will be spurious (*false positives* or Type I error). Therefore, F-score is considered a better method since it takes both aspects into consideration. The formula used here is the traditional called *balanced F-score* and is the harmonic mean of precision and recall.

  $$F\text{-}score = \frac{2 * precision * recall}{precision + recall}$$

- **Receiver Operating Characteristic (ROC)** is a standard measure for the performance of a binary classifier, in our case, whether the edge under consideration is a part of the real network or not. The curve is created by plotting the *true positive rate* (TPR, also known as precision)

against the *false positive rate* (FPR, also known as fallout). False positive rate is the fraction of edges reported to be true but were actually false. When using normalised units, the area under ROC curve (often referred to as simply the AUC, or AUROC) is equal to the probability that a classifier will rank a randomly chosen positive instance higher than a randomly chosen negative one, where the higher ranked sample is considered to be positive. It means that given two edges, out of which one is false, the area under the curve represents the probability that the test will identify the true edge correctly.

The result of each experiment was recorded as a pair of plots capturing the performance of the method. The abscissa denotes the number of edges included in the inferred network, in the order of decreasing metric value. The first plot shows the trend of precision, recall and F-score whereas the second plot is the ROC curve along with the area under the curve.

Due to variation in multiple parameters, the total experiment count crosses 200 and discussing the observations of each here is cumbersome. Therefore, only the significant results pertaining to the conclusions, without overlooking any special trends, are discussed here.

6.3 Results for Pairwise Random Variable based Techniques

For pairwise metrics, experiments were run over all combinations of:

- Number of genes: $N \in \{10, 20, 50, 100\}$
- Length of time-series: $T \in \{500, 1000\}$
- Quantisation levels: $Q \in \{2, 5, 10, 20\}$
- Pairwise metrics: *metrics* $\in \{$*co, gc, mi, te, ccm*$\}$

However, after hundreds of experimental runs, it was realised that larger networks gave the poorest results. Thus, we stick to including results only for $N \in \{50, 100\}$, and $Q = 20$ (quantisation done only for probabilistic methods of transfer entropy and mutual information). (See Section 8.1 for plots.)

Starting from the traditional method of **correlation**, the results were surprising. The area under ROC was close to 0.9 which, near to perfect classifier. However, the peak values of precision and recall was not significantly high and decayed sharply after few edges, which means that the sensitivity and specificity of the method are actually not good.

For **Granger Causality**, the results obtained were bad. The peak value of precision and recall are similar to that of correlation but the decay happens soon and fast. This could be attributed to the fact that GC assumes the variables to be linearly related, which is not true in this case (see Section 3). Therefore, techniques to incorporate non-linearity in the basic Granger-Weiner framework are under research. One such method, causal mutual information (transfer entropy) is explored in this project.

In case of **Mutual Information**, the results obtained are mostly better than Granger causality. The fact that information theory approaches can capture the non-linearity of the system makes them viable options for detection and prediction purposes and mutual information is no exception. The drawback of mutual information, its inability to infer direction, is tried to be compensated by finding the lag value for which the value is maximized and using its sign to interpret the direction. As a result, we observe that the performance of mutual information is higher than GC.

Transfer Entropy was expected to outperform the other three but the results observed are not in agreement with this expectation. Although the precision and recall values for Transfer Entropy was observed to be better than GC and MI in general and the area under the ROC was also higher, it didn't outperform correlation. This verifies the fact that non-linear analogs of GC are indeed a good option for causality prediction and need to be explored more. However, being an information theory approach, binning size is a very important variable when measuring transfer entropy. The performance of the method was affected to a large extent by the quantisation level. We experimented with 10 and 20 quantisation levels. Some performed better for 10 and others for 20. Thus, the method seems promising but there are parameters such as quantisation level which need to be set with extra precaution for the experiments to succeed.

Apart from the above observations, there were certain trends in performance, observed across methods. These were associated to variation in parameters that characterise the data, namely, network size, quantisation level and length of time series data.

- With increase in the **network size**, performance of correlation lightly increased whereas all other pairwise methods show a drop.
- The change of **quantisation level** changes the performance of the information theory methods. The nature of change was not same for all. In case of MI, the results were better for 20 quantisation levels whereas for TE, 10 quantisation levels performed better. One might expect there to be a sweet-spot value of Q where neither the sample space is too large, nor too much quantisation error is induced in the calculations. Figuring an optimal Q is thus very crucial.
- **Length of time series** data did not have any direct implications on the quality of results obtained.

6.4 TE and MI after Laplace Smoothing

For reasons explained in 4.5, Laplace Smoothing (LS) is expected to improve probability estimates in the face of lack of sufficient data. We test this hypothesis: particularly for the probabilistic techniques of Mutual Information and Transfer Entropy.

Clearly, LS has improved the probability estimates, since the AUC has largely improved for both MI and TE, across bin sizes. Especially for a large bin size of 20, where the sample space of the signals would be the largest, the AUROC with LS gives better results across the tested configurations. (As a test, we try this with small networks of sizes 10 and 20, see Figure 10.) This hypothesis of poverty of data can be further tested by using longer time-series data, and then comparing AUROCs with and without LS for MI and TE.

6.5 Results for Pairwise CCM

Evaluating pairwise Convergent Cross Map is fairly time-expensive, due to reconstruction from local neighbourhoods, across shadow manifolds. For all networks, the lag ($\tau = 1, 2$) and dimensionality ($E = 2, 4, 6, 8, 10$) parameters were varied. Note that this metric is different from all others discussed above, in that it doesn't assume a probability distribution for the signals, rather, it assumes a dynamical system instead.

For all configurations, we observe that CCM performs best, next only to correlation. There is high precision initially, at low recall, and it slowly falls down as more links are added. Which is indicating that critical links are really the ones being selected by pairwise CCM as most important. As the time series data of a network increases, we observe that the performance of CCM increases and is almost as good as correlation. One might be able to see the success of CCM compared to information theoretic methods, by thinking about how an increase in data size (time-series length) affects the precision in estimation of model parameters.

We also observed that the performance of CCM increased with time series data. For a dynamical system, the temporal information in encoded within the manifold itself, with smallest of information sufficient to describe a shape of the manifold. Any increase in length only makes the manifold denser and more precise. Thus, there is a sense of an **early start** for convergent cross map. Acquiring data till a certain low threshold is enough to start approaching the true manifold. These are intuitive claims, and remain to be validated with mathematical rigour. Also, this hypothesis can be tested by working with very large time-series data.

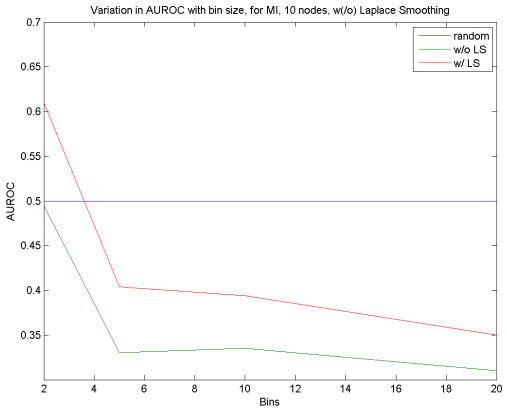

(a) $N = 10$, MI

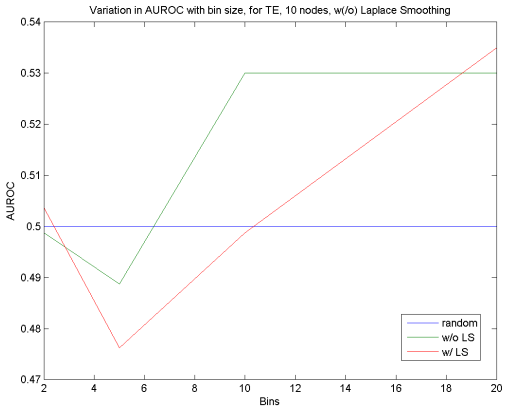

(b) $N = 10$, TE

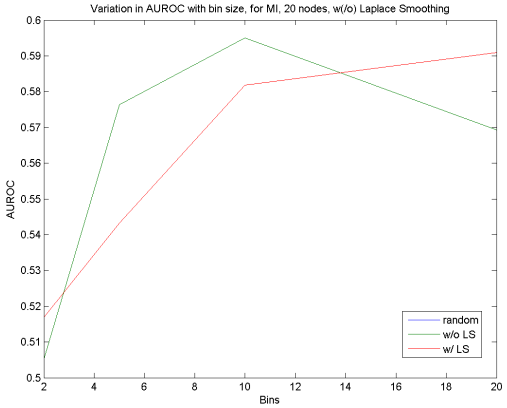

(c) $N = 20$, MI

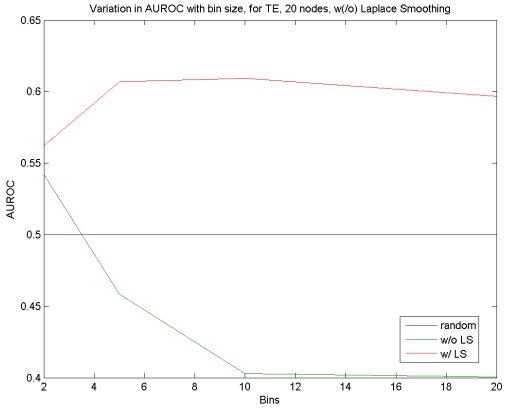

(d) $N = 20$, TE

Figure 10: Variation of AUROC with Quantisation Levels, with Laplace Smoothing.

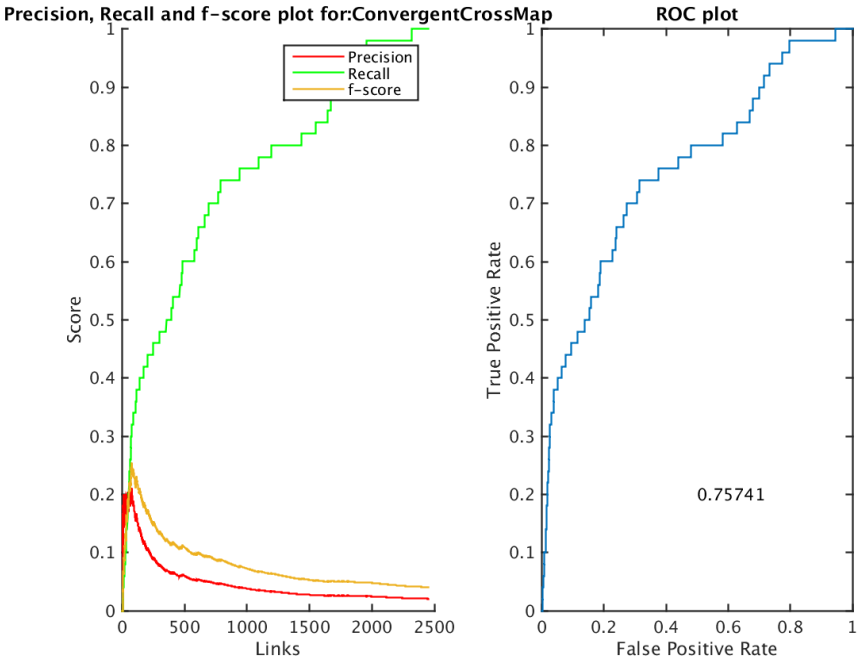

Figure 11: CCM result metrics for $N = 50$, $T = 500$

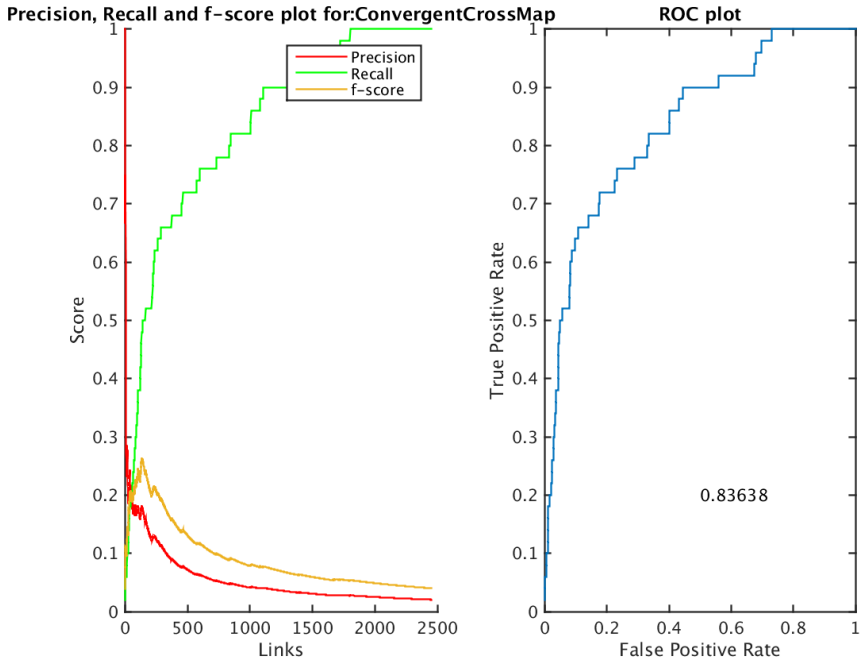

Figure 12: CCM result metrics for $N = 50$, $T = 1000$

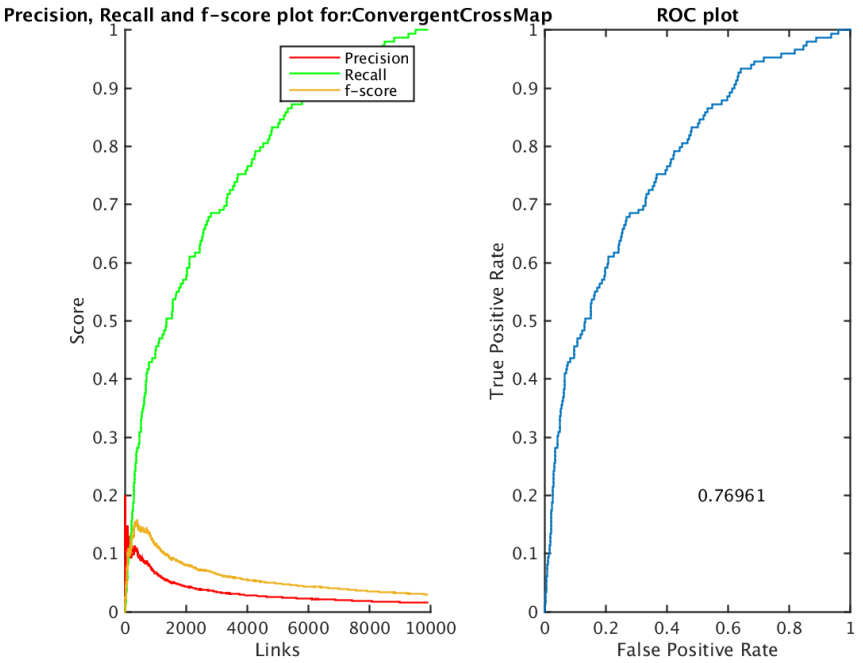

Figure 13: CCM top-k links for $N = 100$, $T = 500$

6.6 Intrinsic Graph Estimation on DREAM4 dataset

Since IGE is computationally very expensive, we choose the smaller 10-node DREAM4 dataset to test it (See Section 2.5). For now, we merely replicate the original IGE formulation of Noda et al., using a single-attribute observation matrix without any regularisation. Since the methods of Correlation, Granger Causality and Convergent Cross Map have come across as better (also they do not require quantisation of data) amongst the pairwise techniques, we include results corresponding to only these metric matrices.

For all the three PW techniques, the AUROC surprisingly lowers when we use IGE, instead of the naive top-k selection strategy (see Figures 14, 15, 16, 17, 18 and 19). For IGE plots, we have also marked the precision, recall and f1-score for to the most optimal (least error) Θ. Evidently, the most optimal Θ doesn't correspond to the one with the highest f1-score either.

Also, we observe that IGE tends to produce somewhat denser networks (see Figures 20 and 21). Although this increases the recall, but the precision actually falls immensely. One way to tackled this is to use regularisation, as described above in Section 5.2.

We are currently in the process of running experiments after applying regularisation, and seeing if the multi-attribute setting improves results. However, the problem in the current algorithm is more than just this:

- The current function f, is the matrix exponential map. Its inverse function, which is critical to estimating Θ, is the matrix logarithmic map. Although the former exists and is always well-defined, the *log* of a real matrix exists if and only if it's invertible (i.e., determinant $\neq 0$). Even if the *log* exists, it is not unique, unless its eigenvalues lie in the strip $\{z \in \mathbb{C} | -\pi < Im(z) < \pi\}$. The unique *log* is called the principal logarithm. However, since it may not be unique, the inverse map could map to an entirely different Θ. Thus, one possible direction of further work is to choose another function which satisfies the random walk model.

- We have employed MATLAB's *fminsearch* function to solve the unconstrained optimisation problem in minimising the error function. Despite increasing the option of maximum function evaluations and maximum number of iterations, a few times the function returns without reaching the optima. This is possibly because the error landscape is more complicated that a simple convex function, and/or the starting point of initialisation of parameters ρ (which is being drawn from a random number between 0 and 1) is too far off from the minima.

Another concern is the density of most optimal Θ being returned by IGE. As seen in Figures 8 and 9, there are some significant differences in how the error varies with the size (in terms of number of detected edges) of the network. Correlation and GC tend to favour denser networks, while CCM favours sparser networks, something which makes CCM more suited towards an IGE type of analysis, if we are to not use any form of regularisation.

We have also enclosed results of IGE analysis on large synthetic datasets (see Section 8.2 for the plots). However, the results on large networks are very poor. Thus, a lot of further work needs to be done before declaring intrinsic graphic estimation a success in creating a global causal model for GRNs.

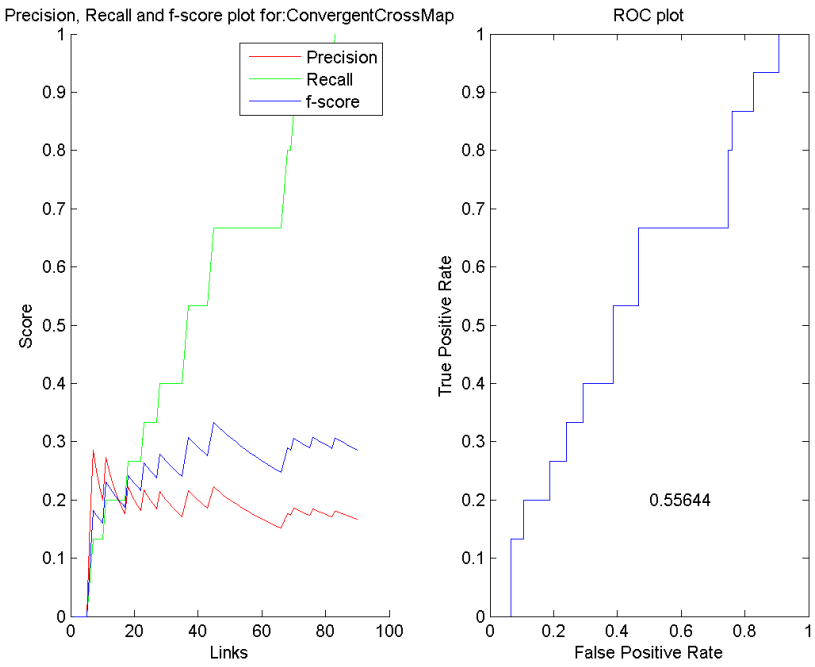

Figure 14: Pairwise CCM

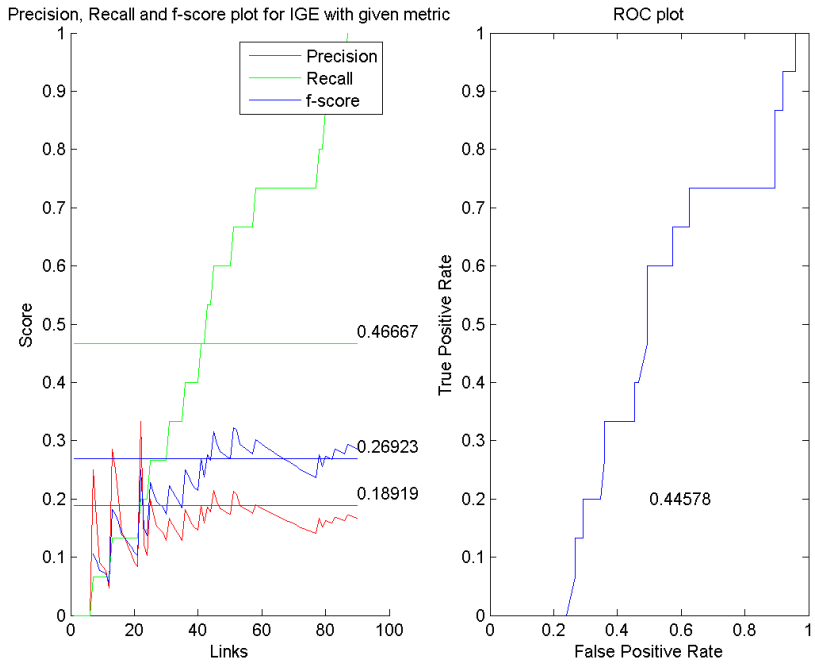

Figure 15: IGE (simple) with CCM Metric Matrix

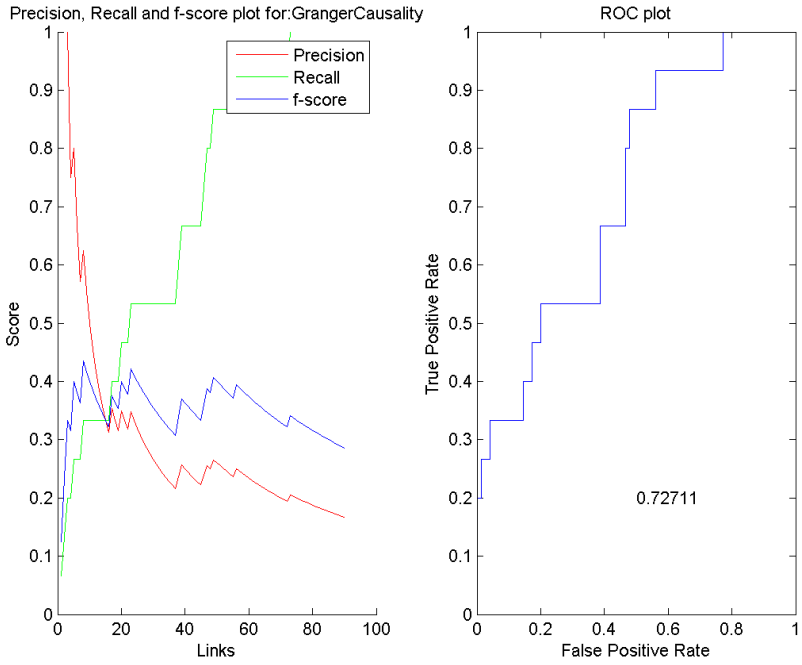

Figure 16: Pairwise GC

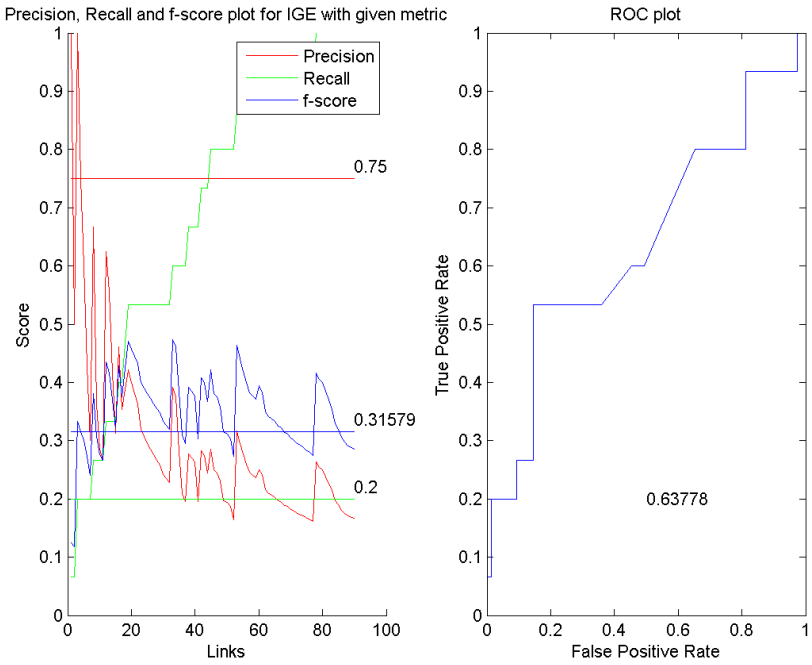

Figure 17: IGE (simple) with GC Metric Matrix

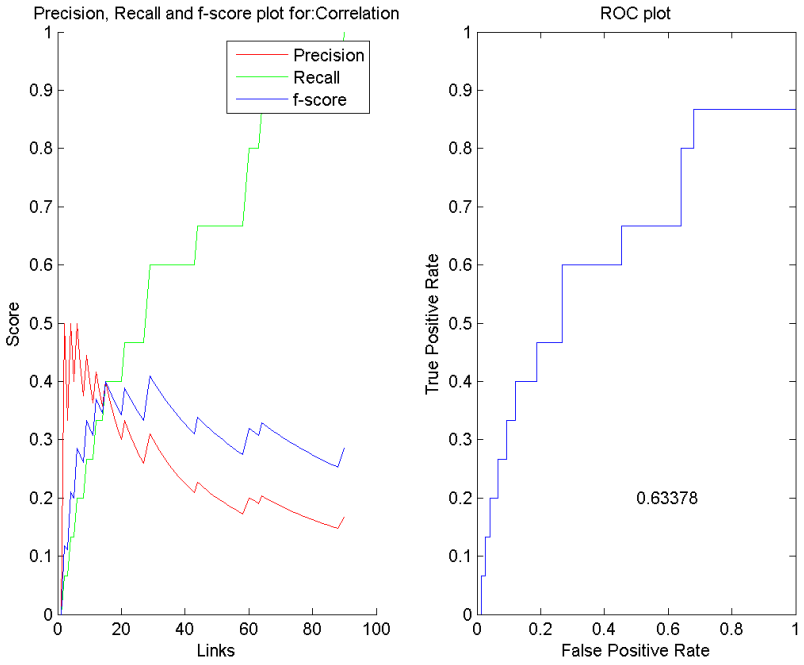

Figure 18: Pairwise CO

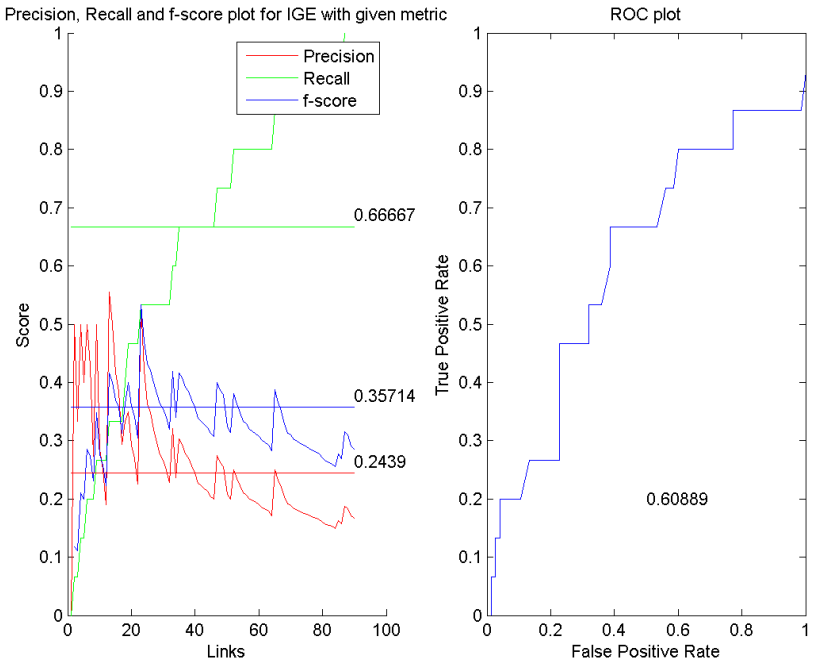

Figure 19: IGE (simple) with CO Metric Matrix

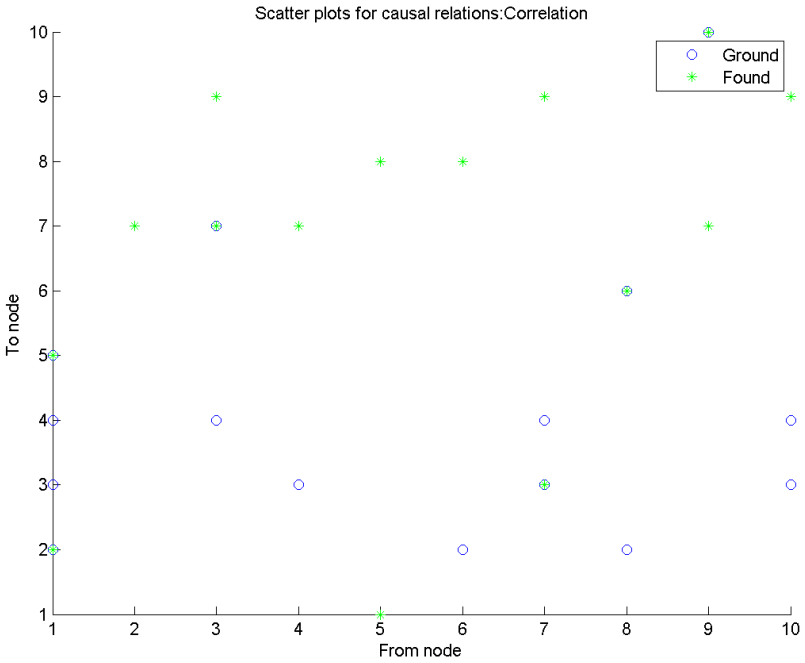

Figure 20: Scatter plot of top-k found edges for Pairwise CO

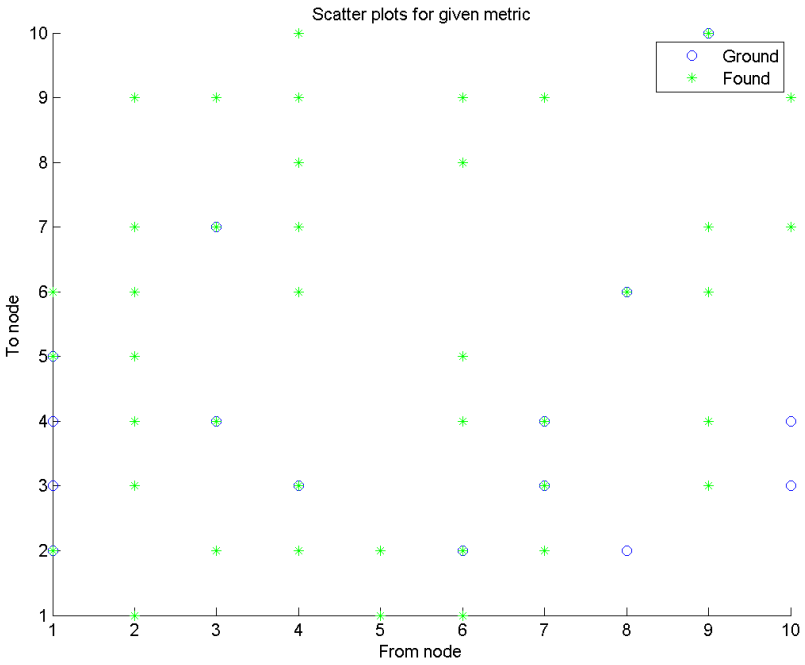

Figure 21: Scatter plot for edges found by IGE (simple) with CO Metric Matrix

6.7 ARACNE on large synthetic datasets

In order to compare our results with those of popular network finding methods, we tested the performance of ARACNE on our datasets. It works by estimating MI values, thresholding on the basis of p-value, and then using DPI to further remove false edges. To create ROCs, we executed the following strategy. We first generated the complete MI matrix for all networks by setting p-value as 1 and DPI value as 0, indicating that no pruning is done. Then, we varied DPI from 0 to 1, with a step size of 0.01, maintaining the same p-value of 1, so that the parameter being tuned is the DPI tolerance.

The results were similar to traditional precision recall curves (see Figures 22 to 25). The AUROC is lower than only one method of ours, the simplest pairwise correlation, but the peaks of precision and recall is almost double of the other methods. This proves the reliability of the method in picking up true edges fast. The results pertaining to different networks with ARACNE are shown below.

Clearly, ARACNE outperforms our global optimisation method of IGE at the moment. Further work needs to be done to explore why this is the case.

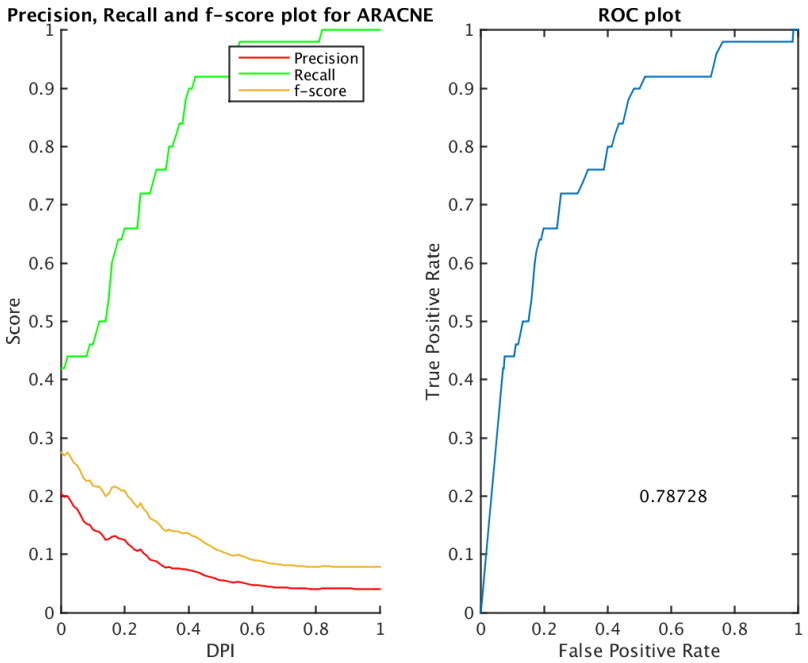

Figure 22: Performance of ARACNE for $N = 50$, $T = 500$

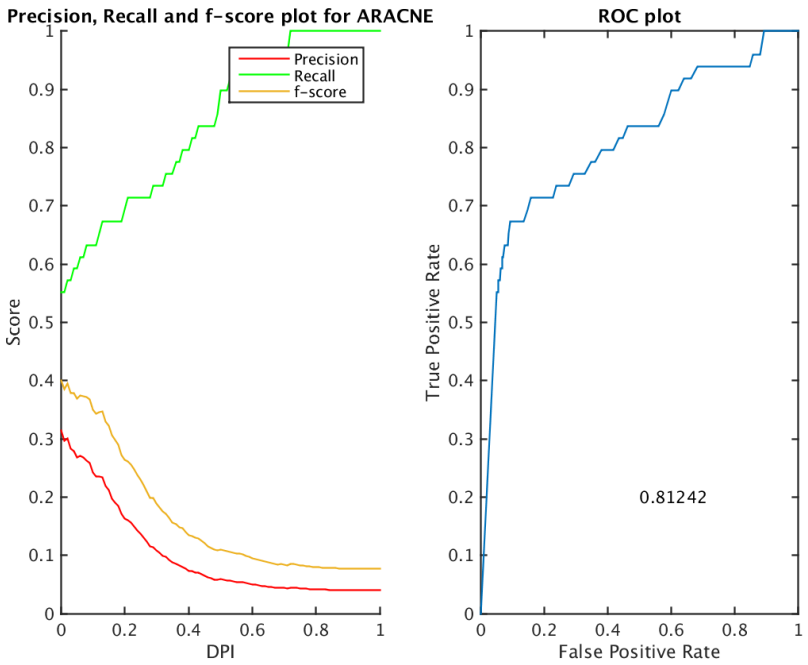

Figure 23: Performance of ARACNE for $N = 50$, $T = 1000$

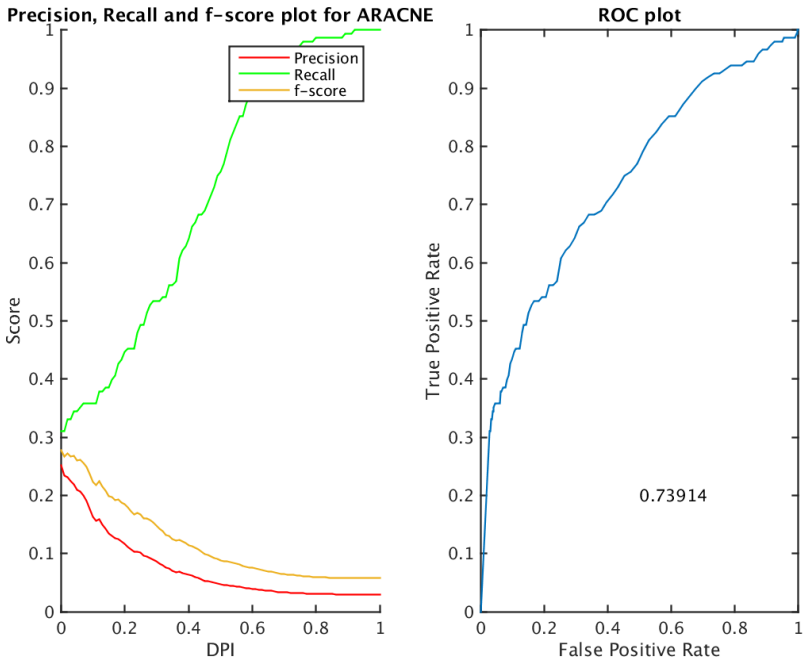

Figure 24: Performance of ARACNE for $N = 100$, $T = 500$

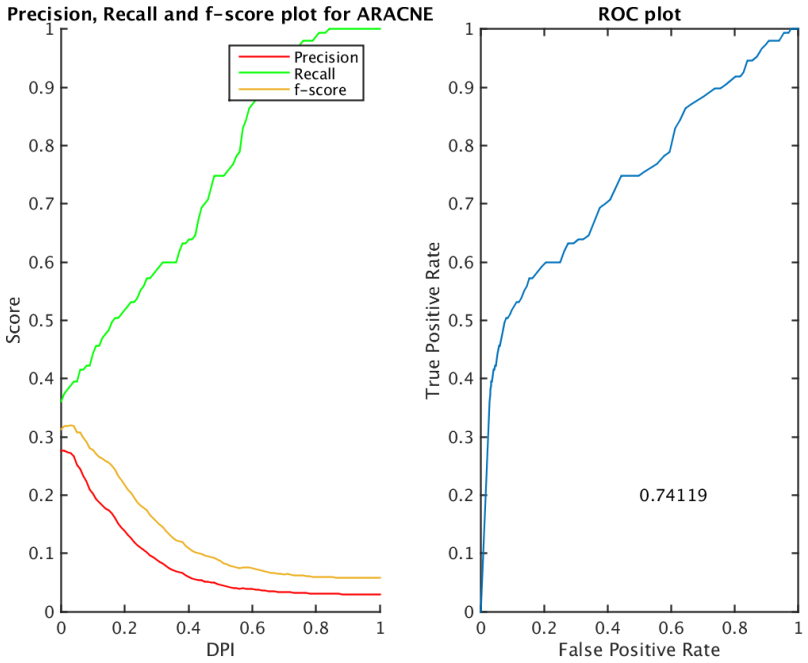

Figure 25: Performance of ARACNE for $N = 100$, $T = 1000$

7 Summary and Future Work

This project was an attempt to review current literature, spanning domains of gene regulatory networks, biological network inference and causality detection and estimation. We started out with investigating methods which would look at pairwise levels of interaction to detect and quantify the existence of a causal relation. After a thorough review, we employed five techniques for this.

Correlation, Granger Causality, Mutual Information and Transfer Entropy are four methods which treat time-series signals as a random variable, following some underlying probability distribution. While the first two work for linear systems, the latter two for non-linear, GC and TE can principally distinguish between the two directions of causality. However, TE and MI suffer from the issue of poverty of data, since they make use of joint probabilities over a large sample space. Thus, Laplace Smoothing was used to smooth the data for these methods, which showed significant improvements. But surprisingly so, the ultimate winner of these techniques was correlation. After running multiple experiments, we observe a soft trend of $CO > TE > MI \approx GC$.

Additionally, one method which seems to outrun all of these (but correlation) was of convergent cross map. This metric assumes the signals as belonging to a dynamical system. It is indifferent to the (non-)linearity of the system, and respects the direction of causality as well. Our experiments show significant increase in performance, making it the most suitable candidate to detect and estimate pairwise causality, alongside correlation.

$$CO > CCM > TE > MI \approx GC$$

However, this is far from developing causal models of entire gene regulatory networks. In all likelihood, the problem of GRN discovery is currently underconstrained, if we stick to looking at only pairwise interactions. Thus, we moved to a global optimisation scheme of intrinsic graph estimation. However, in its simplest single-attribute form, it gives results slightly poorer than pairwise techniques. Thus, there is a need to improve this by using more than one metric matrix at a time, and introducing some kind of a regularisation. Moreover, the algorithm for IGE itself needs further improvement, in terms of deciding a functional map f with a unique inverse.

Furthermore, GRNs consist of genes influencing behaviour of other genes, both upstream and downstream. One could imagine characterising a **local vicinity of influence** over which these methods of causality are employed. Moreover, various **global properties** of biological networks, such as their scale-free nature, average path lengths, observance of Data Processing Inequality as in ARACNE, etc. can also help in constraining the causal computational model. Although we have moved towards a method of global optimisation, a trade off between local structures and global structures is expected to improve the results many fold.

8 Appendix

8.1 Figures for Pairwise Metrics

8.1.1 Results for $N = 50$, $T = 500$

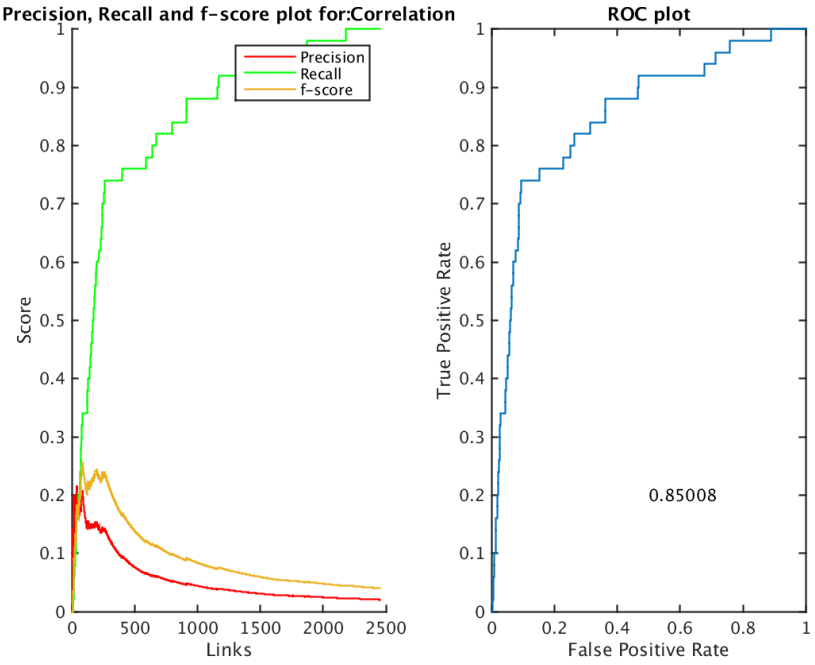

Figure 26: Result metrics for Correlation

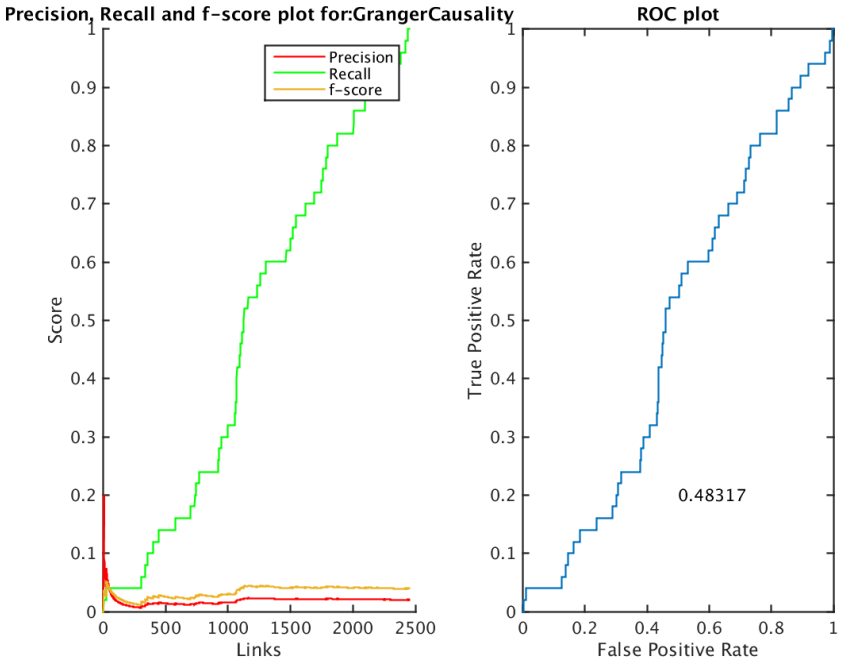

Figure 27: Result metrics for Granger Causality

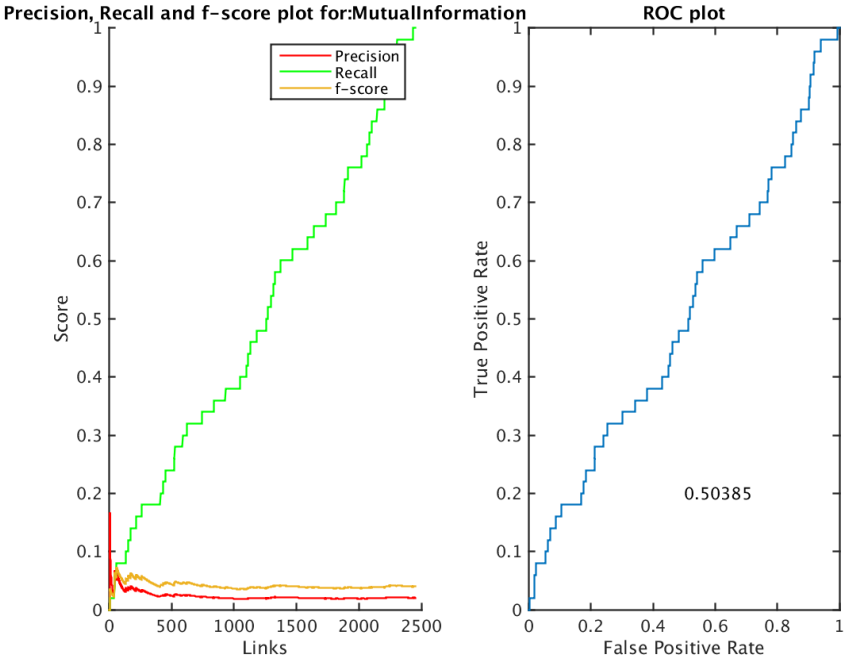

Figure 28: Result metrics for Mutual Information, $Q = 20$

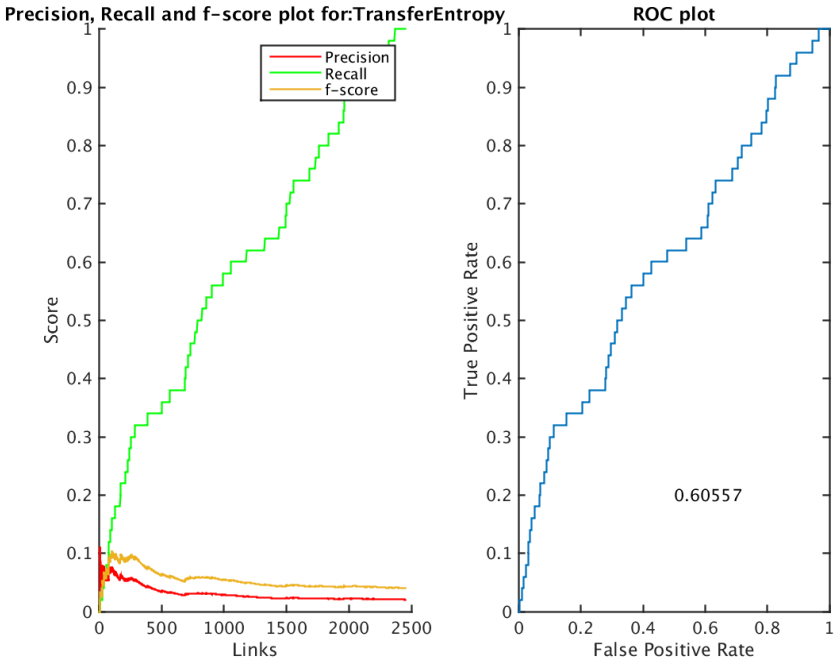

Figure 29: Result metrics for Transfer Entropy, $Q = 20$

8.1.2 Results for $N = 50$, $T = 1000$

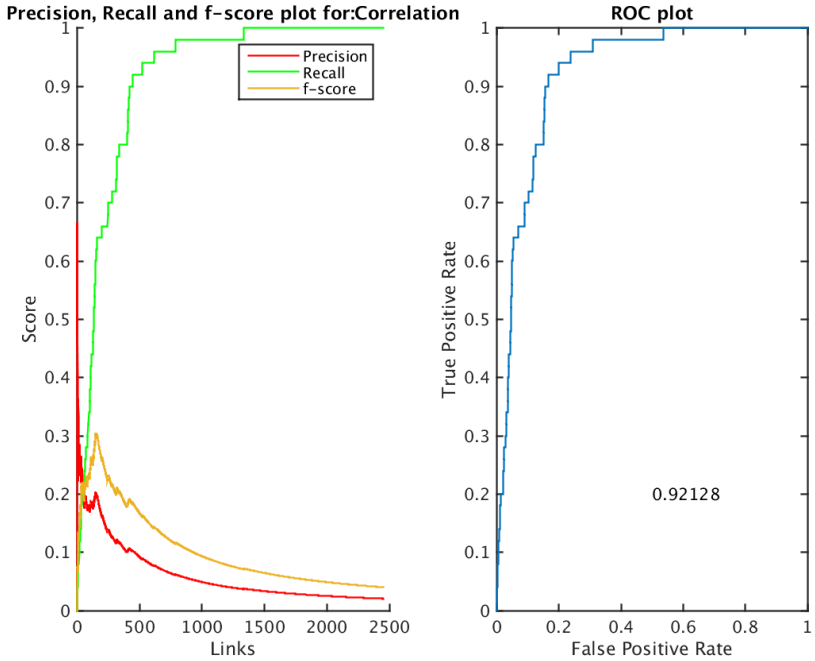

Figure 30: Result metrics for Correlation

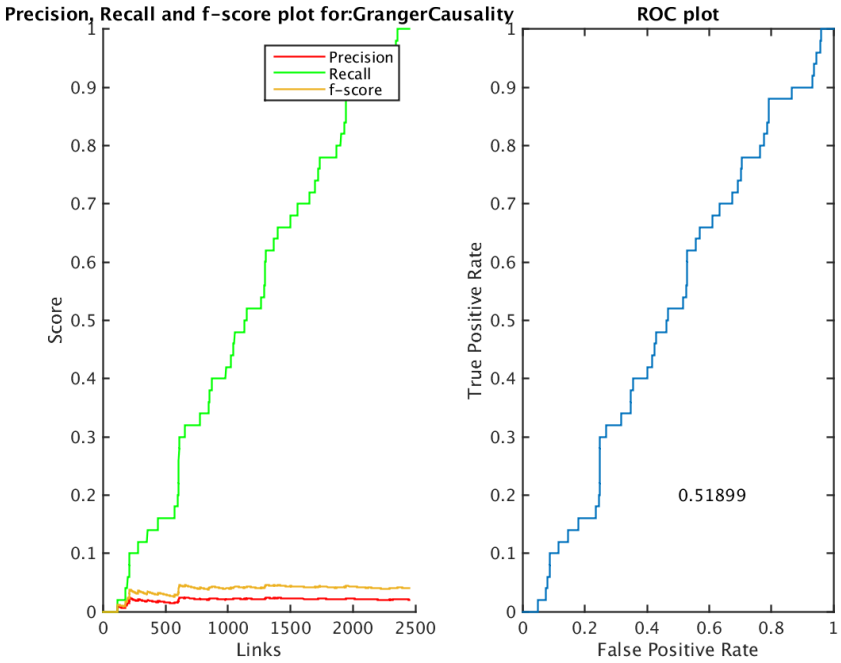

Figure 31: Result metrics for Granger Causality

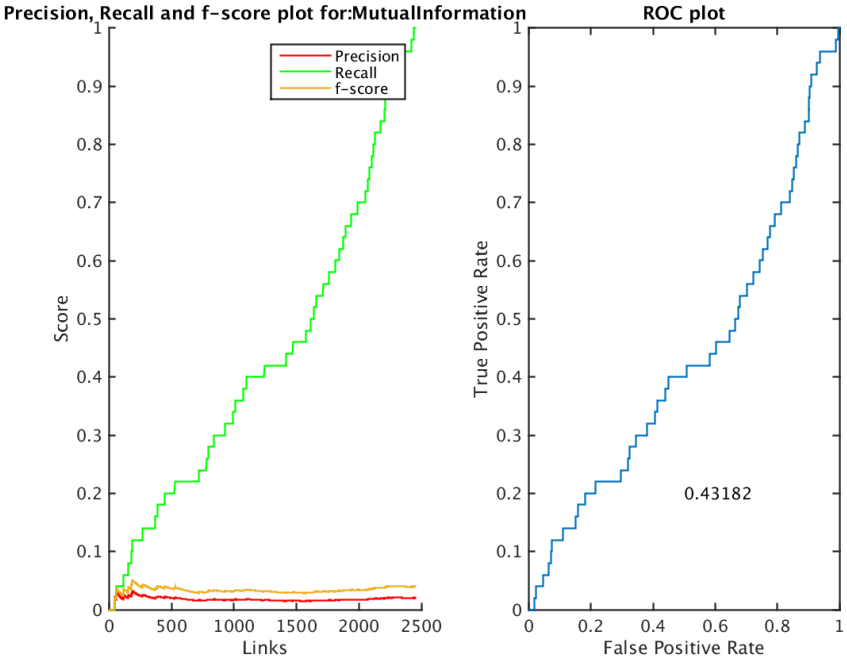

Figure 32: Result metrics for Mutual Information, $Q = 20$

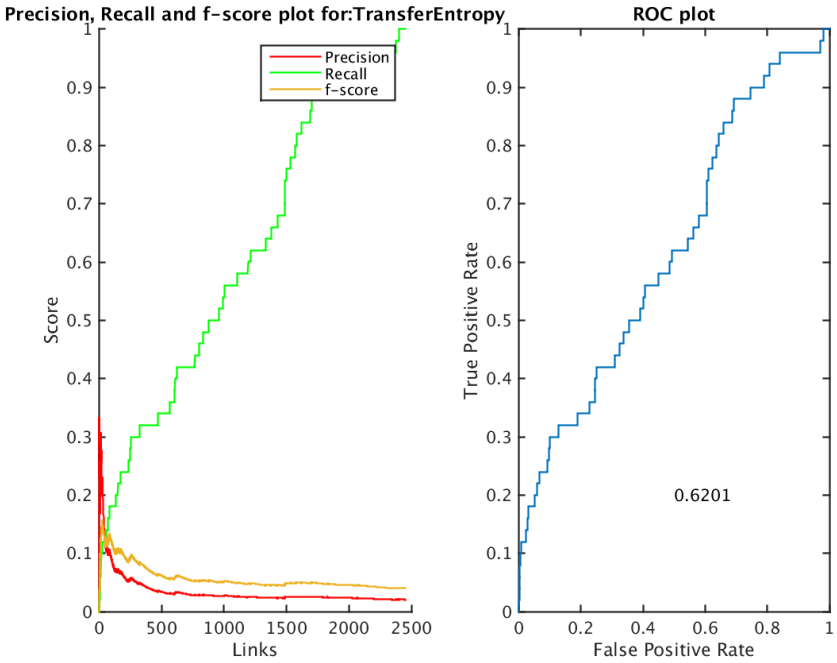

Figure 33: Result metrics for Transfer Entropy, $Q = 20$

8.1.3 Results for $N = 100$, $T = 500$

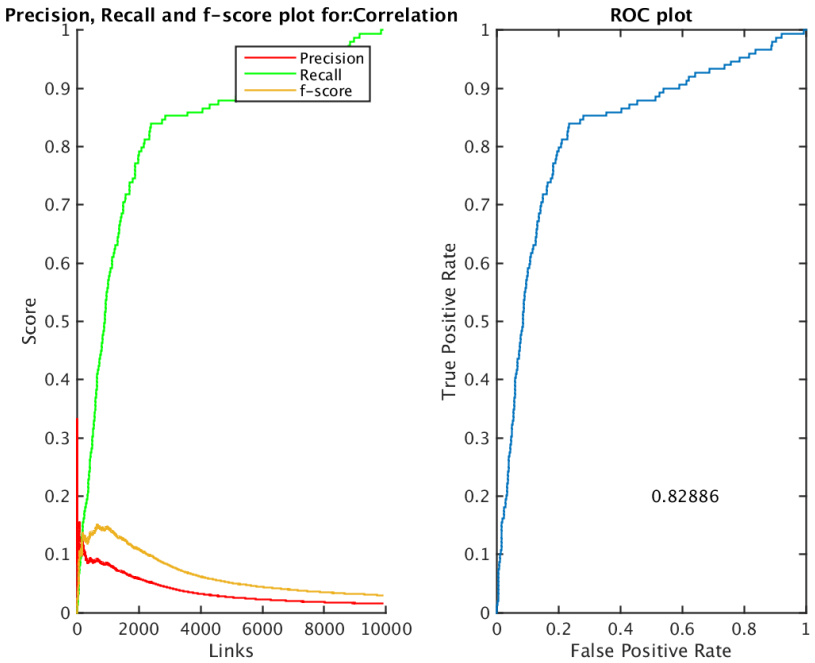

Figure 34: Result metrics for Correlation

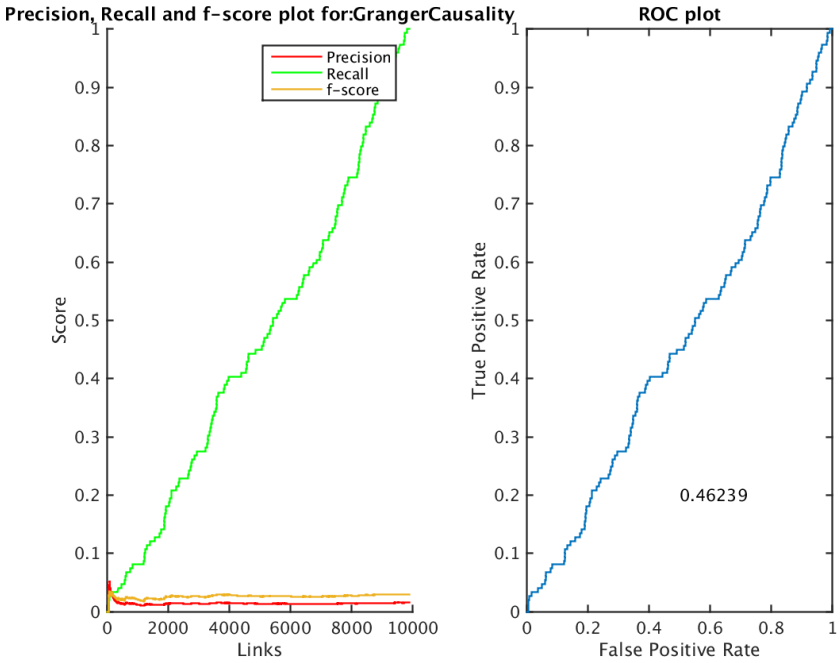

Figure 35: Result metrics for Granger Causality

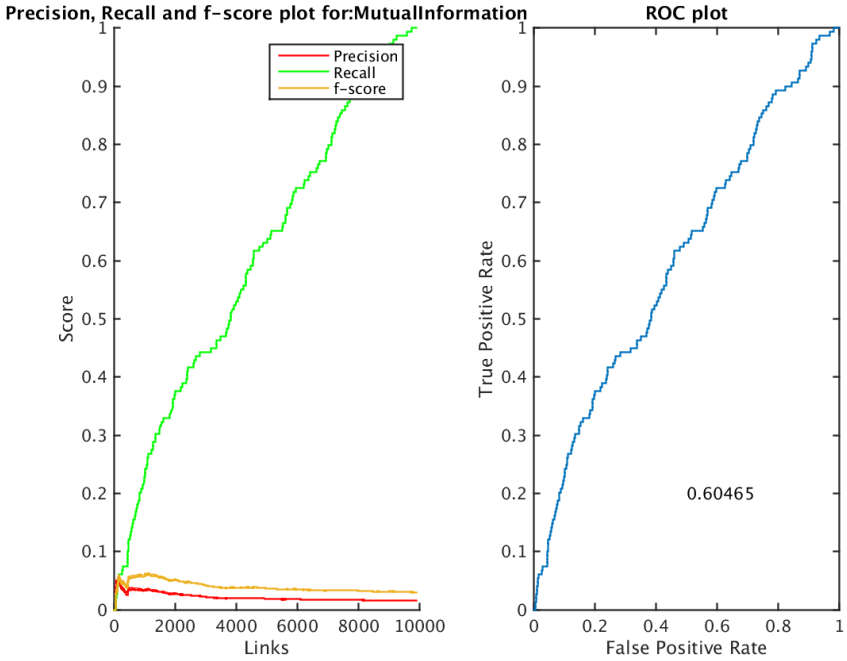

Figure 36: Result metrics for Mutual Information, $Q = 20$

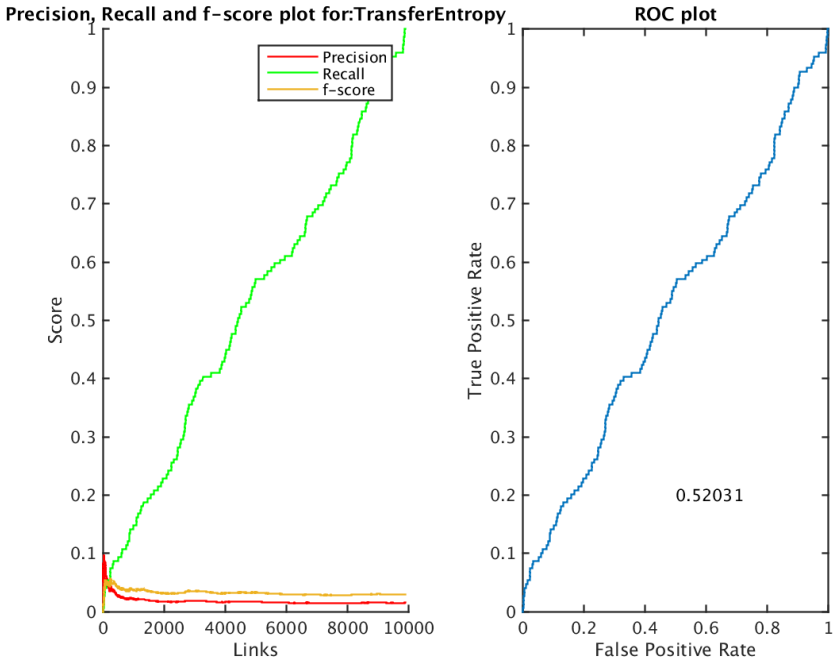

Figure 37: Result metrics for Transfer Entropy, $Q = 20$

8.1.4 Results for $N = 100$, $T = 1000$

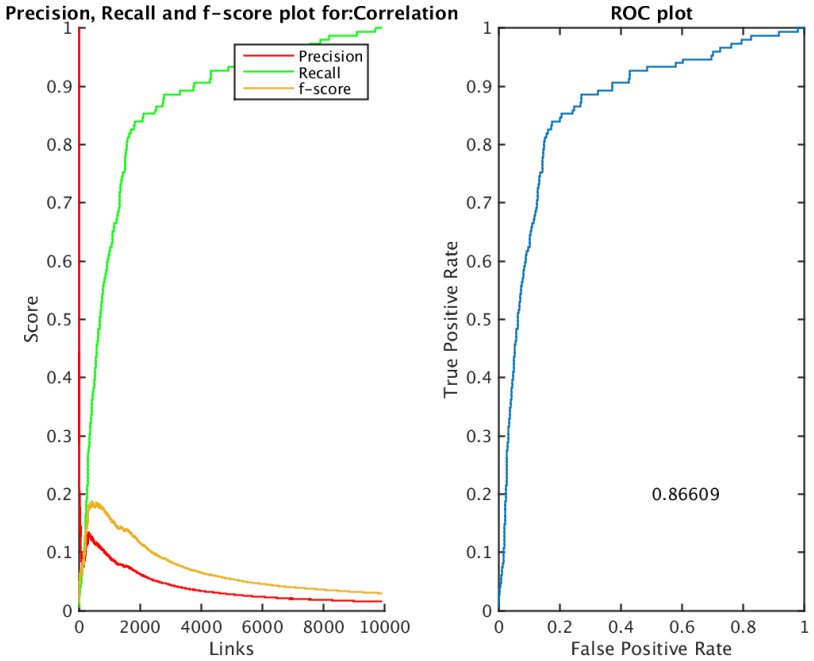

Figure 38: Result metrics for Correlation

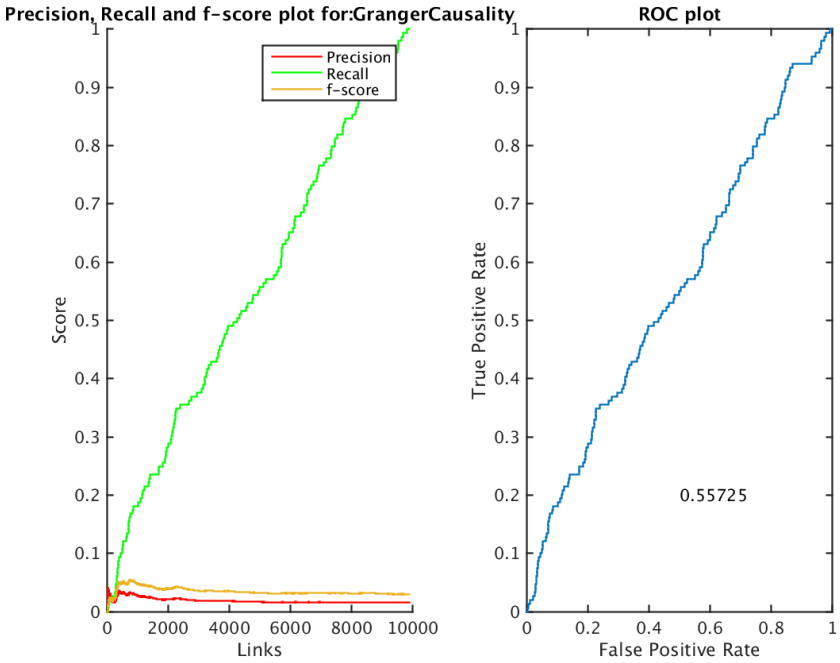

Figure 39: Result metrics for Granger Causality

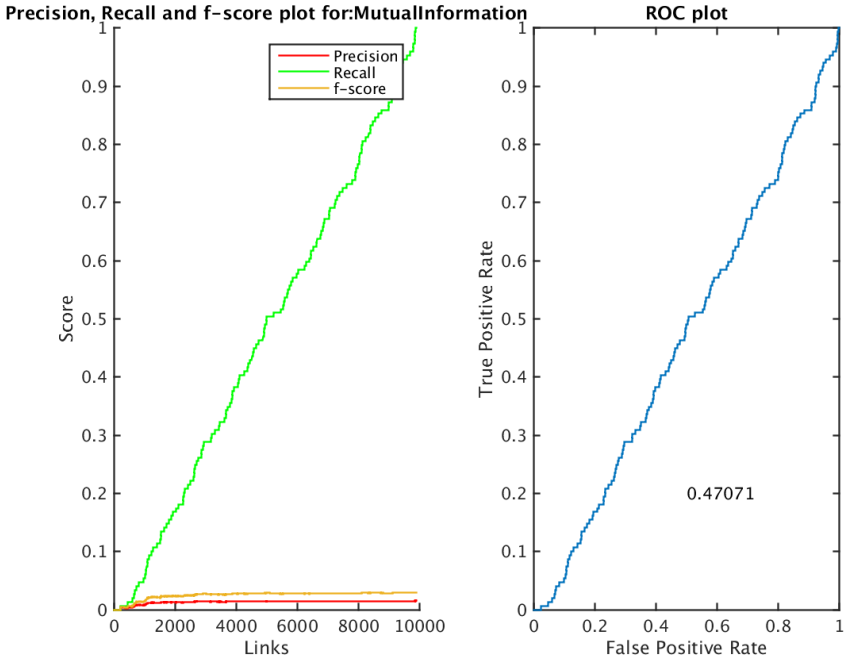

Figure 40: Result metrics for Mutual Information, $Q = 20$

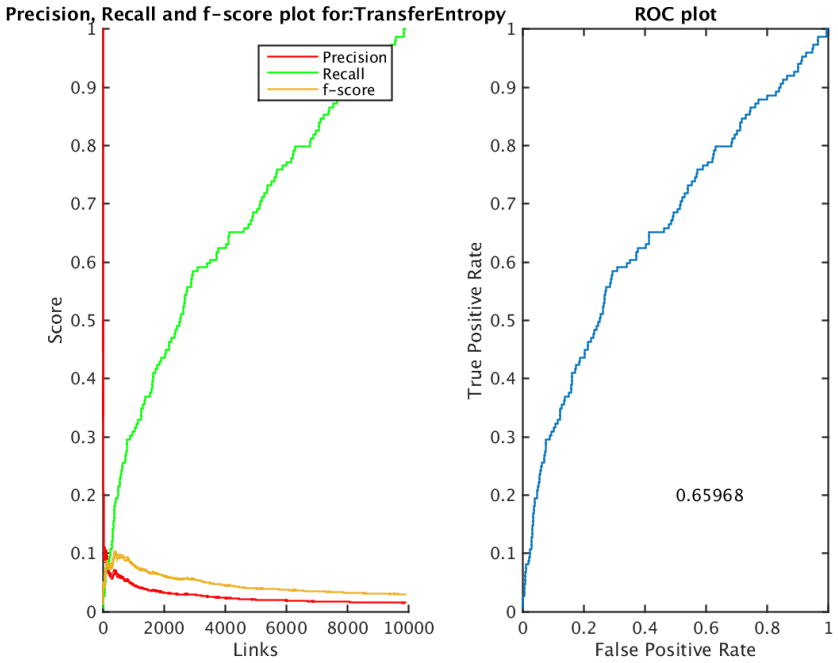

Figure 41: Result metrics for Transfer Entropy

8.2 Figures for IGE Analysis

8.2.1 Results for $N = 50$, $T = 500$

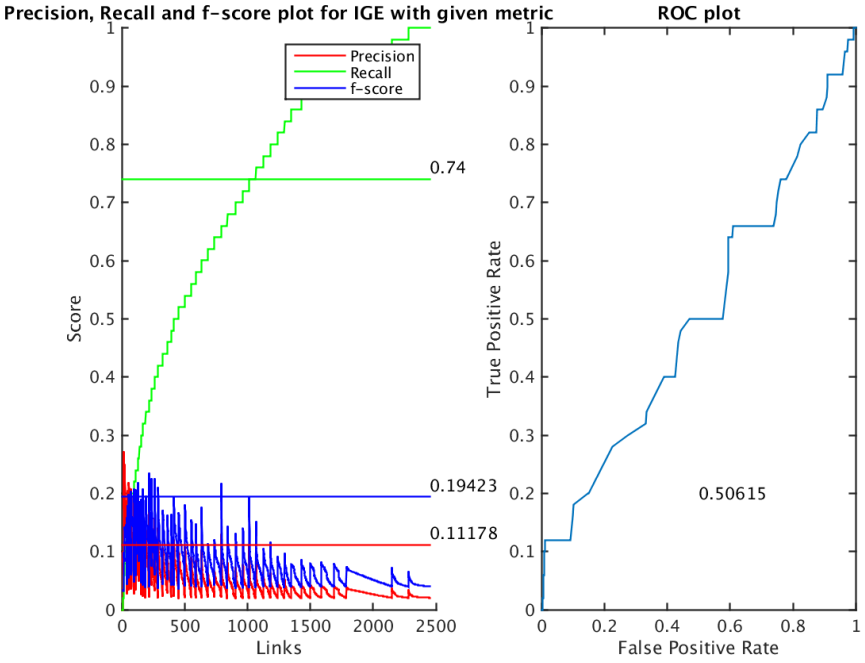

Figure 42: Result metrics for Correlation

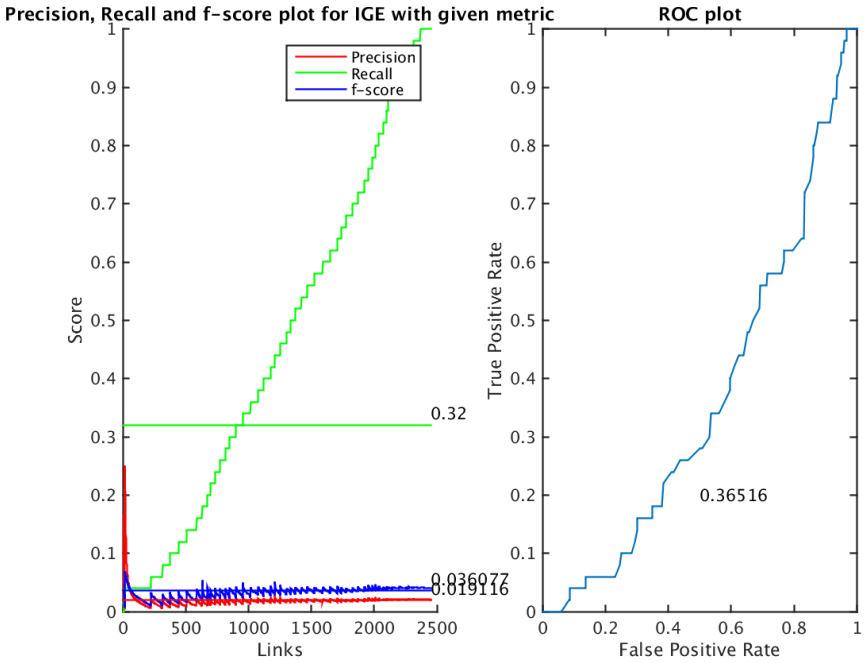

Figure 43: Result metrics for Granger Causality

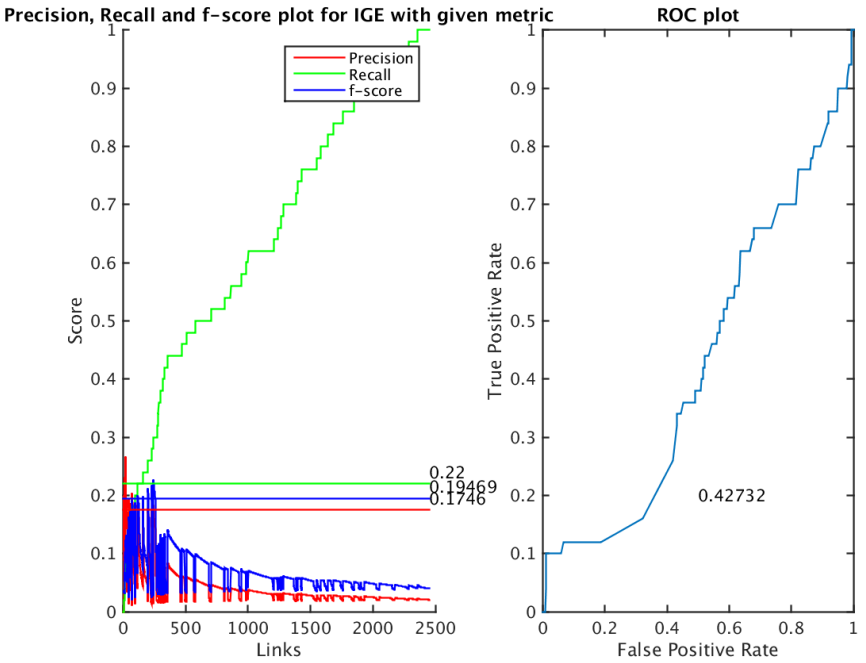

Figure 44: Result metrics for Convergent Cross Map

8.2.2 Results for $N = 50$, $T = 1000$

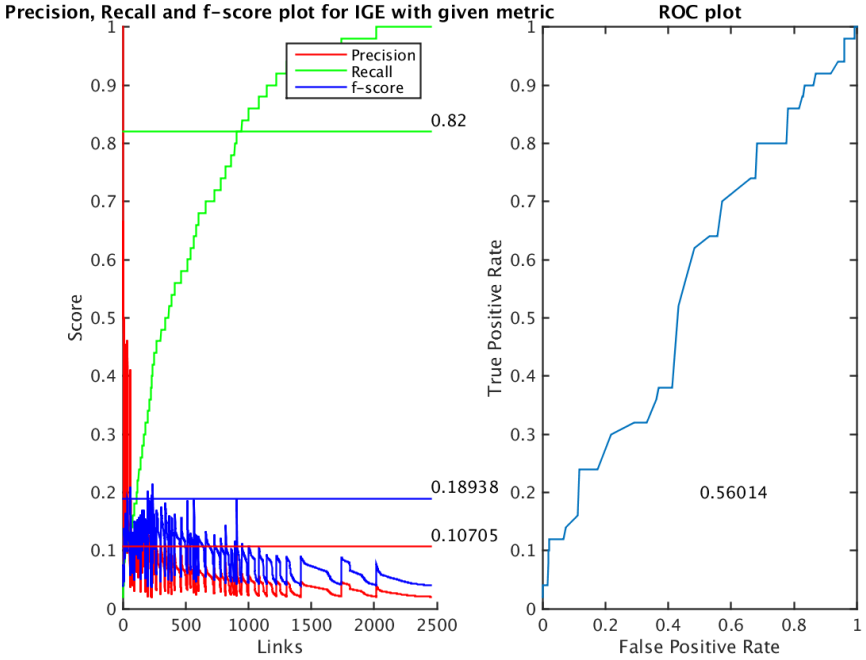

Figure 45: Result metrics for Correlation

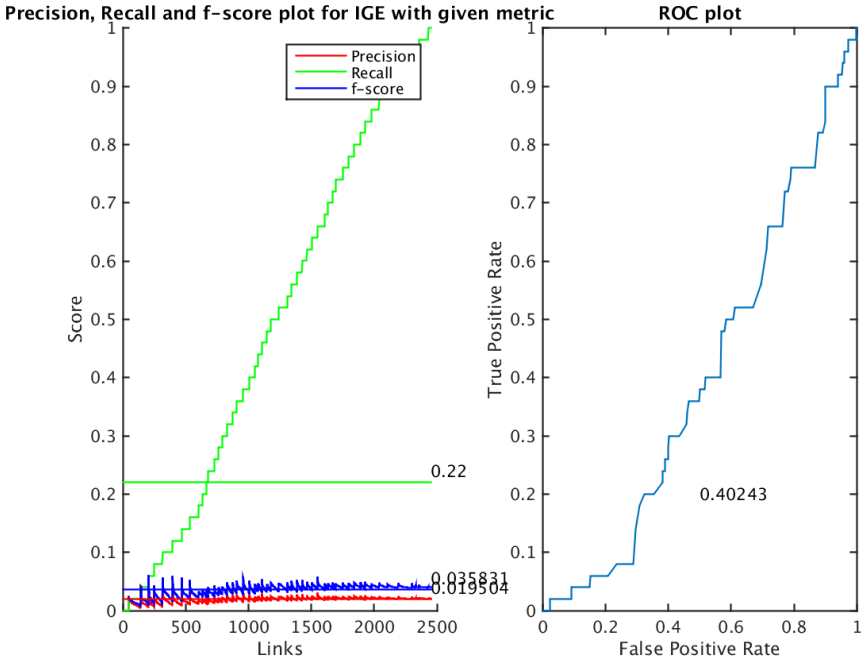

Figure 46: Result metrics for Granger Causality

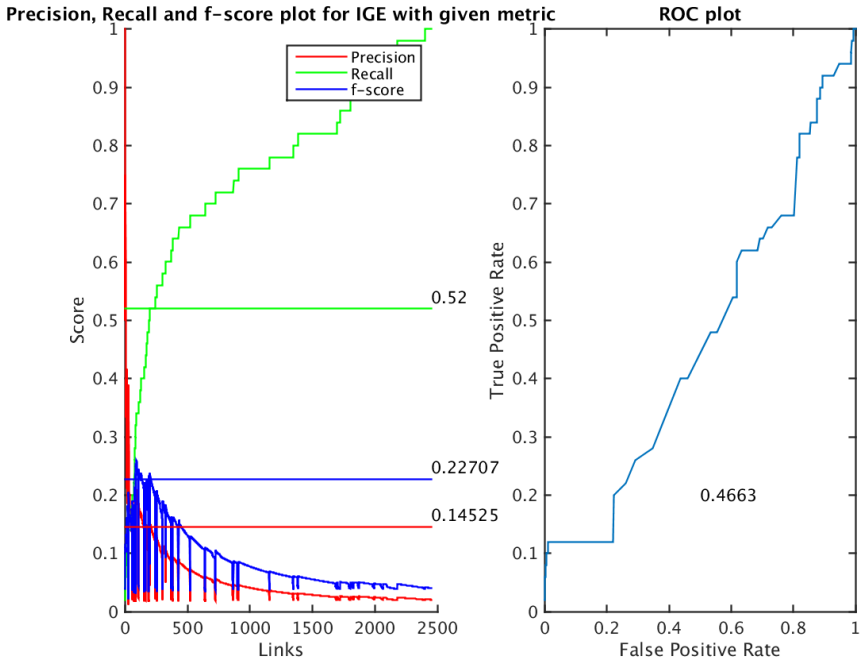

Figure 47: Result metrics for Convergent Cross Map

8.2.3 Results for $N = 100$, $T = 500$

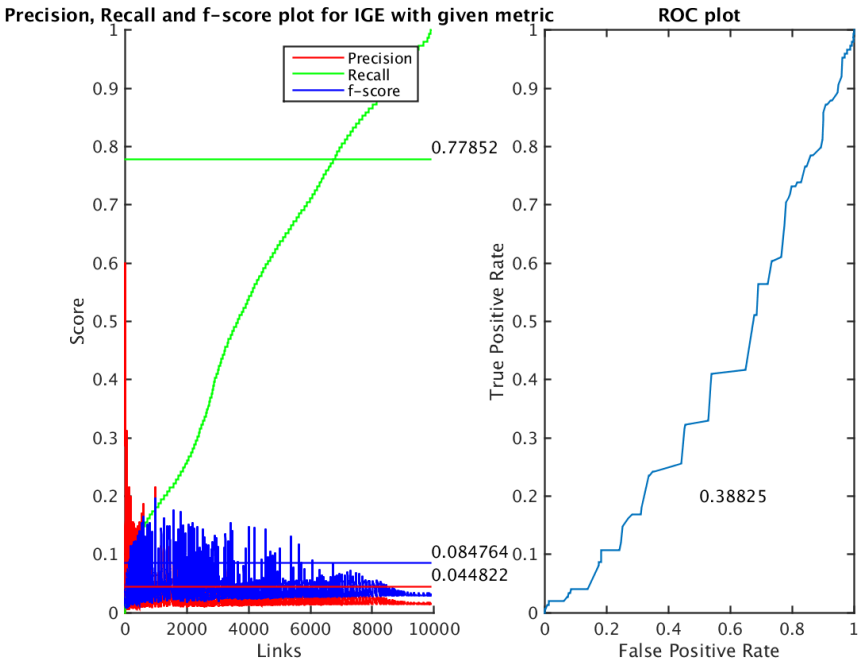

Figure 48: Result metrics for Correlation

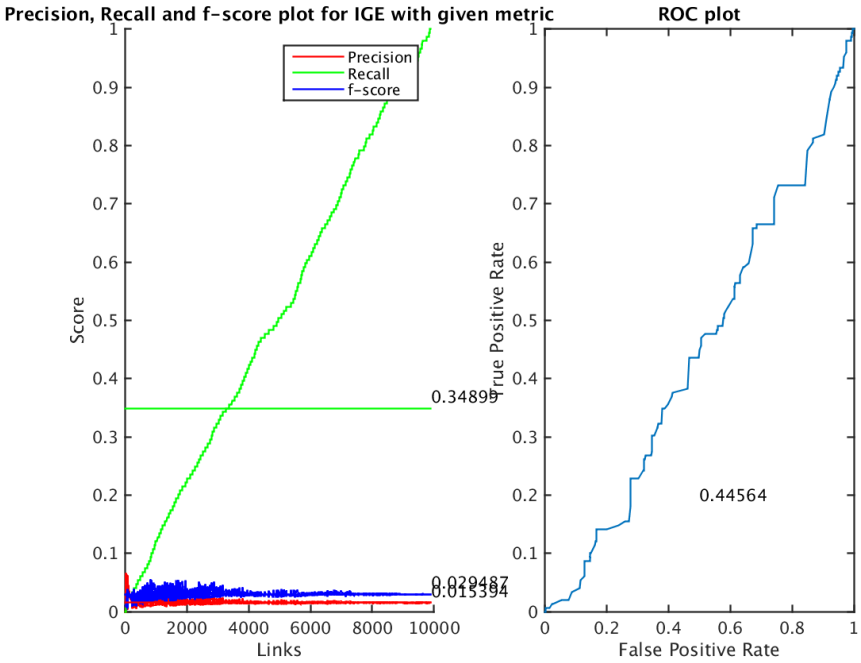

Figure 49: Result metrics for Granger Causality

References

[1] Frank Emmert-Streib, Matthias Dehmer, and Benjamin Haibe-Kains, *Gene regulatory networks and their applications: understanding biological and medical problems in terms of networks*, Front Cell Dev Biol., 2014, 2: 38

[2] Gary Hak Fui Tam, Chunqi Chang, and Yeung Sam Hung, *Gene regulatory network discovery using pairwise Granger causality*, IET Syst. Biol., 2013, Vol. 7 Iss. 5, pages 195–204

[3] Katerina Hlaváčková-Schindler, Milan Palušb, Martin Vejmelkab and Joydeep Bhattacharyaa, *Causality detection based on information-theoretic approaches in time series analysis*, Physics Reports 441 (2007) 1– 46

[4] Adam A Margolin, Ilya Nemenman, Katia Basso, Chris Wiggins, Gustavo Stolovitzky, Riccardo Dalla Favera and Andrea Califano, *ARACNE: An Algorithm for the Reconstruction of Gene Regulatory Networks in a Mammalian Cellular Context*, BMC Bioinformatics 2006, 7(Suppl 1):S7

[5] Young, William C., Adrian E. Raftery, and Ka Y. Yeung *Fast Bayesian inference for gene regulatory networks using ScanBMA*, BMC systems biology 8.1 (2014): 47

[6] Andrea Pinna, Nicola Soranzo, Ina Hoeschele and Alberto de la Fuente, *Simulating systems genetics data with SysGenSIM*, Bioinformatics, Vol. 27 No. 17, 2011, pages 2459–2462

[7] C. W. J. Granger, *Investigating Causal Relations by Econometric Models and Cross-spectral Methods*, Econometrica, Vol. 37 No. 3, 1969, pages 424-438

[8] George Sugihara et al., *Detecting Causality in Complex Ecosystems*, Science, Vol. 338, 2012, pages 496-500

[9] Gideon Schwarz, *Estimating the Dimension of a Model*, The Annals of Statistics, Vol. 6 No. 2, 1978, pages 461-464

[10] Noda, Hino, Tatsuno, Akaho and Murata, *Intrinsic graph structure estimation using graph Laplacian*, Neural Comput. 2014, 26(7), pages 1455-1483